Assessing the Fate of Superparamagnetic Iron Oxide

Nanoparticles Carrying Usnic Acid as Chemical Cargo on the Soil

Microbial Community

4

3

1

2

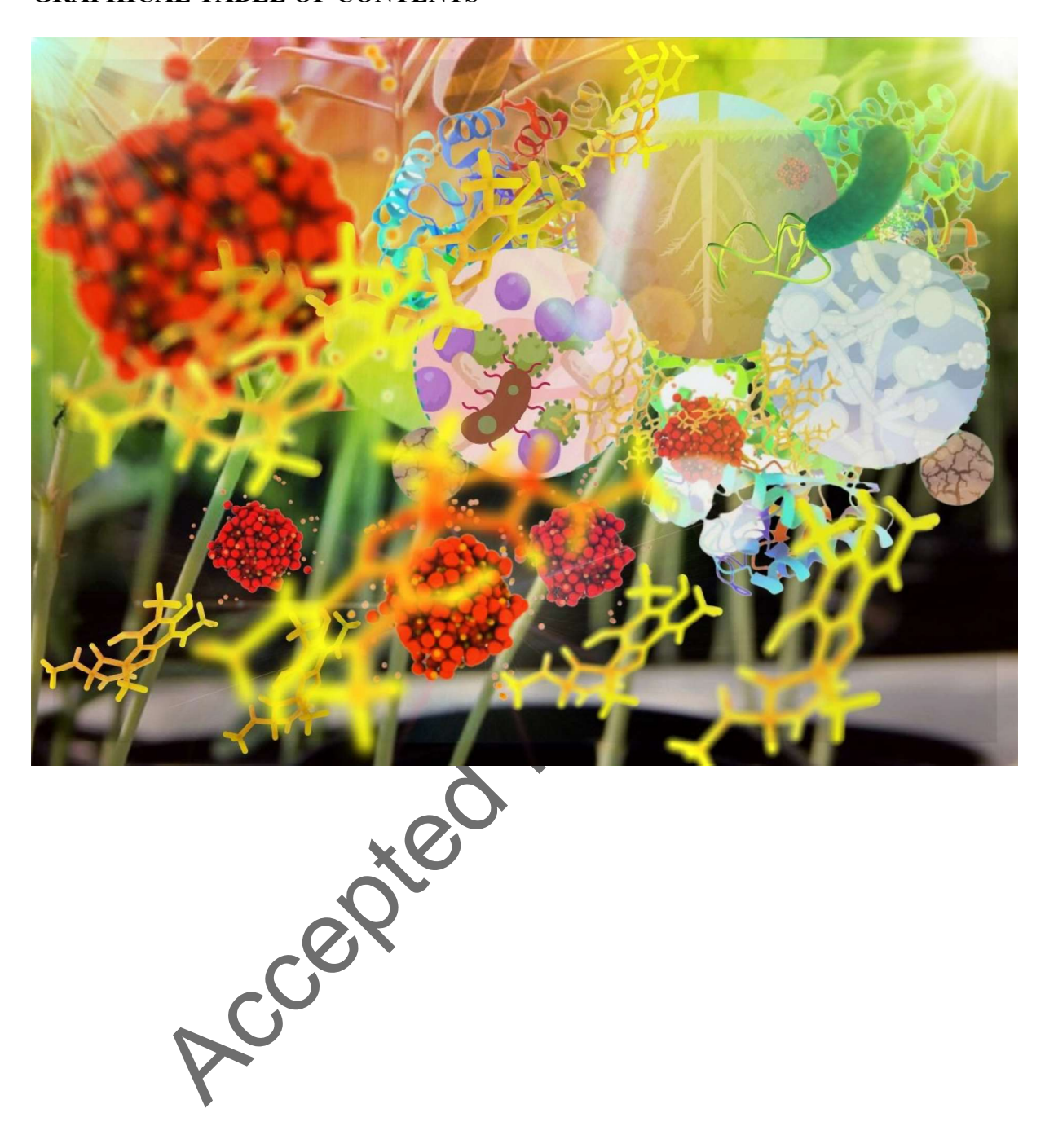
- Montcharles S. Pontes ^{a,b*}, Jaqueline Silva Santos ^c, José Luiz da Silva ^d, Thaiz B.A.R. Miguel
- 6 ^e, Emilio Castro Miguel ^f, Antonio G. Souza Filho ^g, Flavio Garcia ^h, Sandro Marcio Lima ^a,
- 7 Luís Humberto da Cunha Andrade ^a, Gilberto J. Arruda ^a, Renato Grillo ⁱ, Anderson R.L. Caires
- 8 b, and Etenaldo Felipe Santiago a*

9

- ^a Natural Resources Program, Center for Natural Resources Study (CERNA), Mato Grosso do
- 11 Sul State University (UEMS), Dourados, 79804-970, Brazil
- 12 b Optics and Photonics Group, Institute of Physics, Federal University of Mato Grosso do Sul
- 13 (UFMS), Campo Grande, 79070-900, Brazil
- ^c Genetics Department, Luiz de Queiroz College of Agriculture (ESALQ), University of São
- 15 Paulo (USP), Piracicaba, 13418-900 Brazil
- d Department of Analytical, Physico-Chemical and Inorganic Chemistry, Institute of Chemistry,
- 17 São Paulo State University (UNESP), Araraquara, 14800-060, Brazil
- ^e Laboratory of Biotechnology, Department of Food Engineering (DEAL), Federal University
- 19 of Ceará (UFC), Fortaleza, 60440-554, Brazil
- 20 f Laboratory of Biomaterials, Department of Metallurgical and Materials Engineering, Federal
- 21 University of Ceará (UFC), Fortaleza, 60440-554 Brazil
- ^g Department of Physics, Federal University of Ceará (UFC), Fortaleza, 60440-554 Brazil.
- ^h Brazilian Center for Research in Physics, Urca, Rio de Janeiro, 22290-180, Brazil
- ¹ São Paulo State University (UNESP), Department of Physics and Chemistry, School of
- 25 Engineering, Ilha Solteira, SP 15385-000, Brazil

- ^{*}Corresponding authors:
- 28 Etenaldo F. Santiago, E-mail: felipe@uems.br
- 29 Montcharles S. Pontes, E-mail: montcharles@protonmail.com

GRAPHICAL TABLE OF CONTENTS



ABSTRACT

33

In the present study we evaluate the effect of superparamagnetic iron oxide nanoparticles 34 (SPIONs) carrying usnic acid (UA) as chemical cargo on the soil microbial community in a 35 dystrophic red latosol (oxysol). Herein, 500 ppm of UA or SPIONs-framework carrying UA 36 were diluted in sterile ultrapure deionized water and applied by hand sprayer on the top of the 37 soil. The experiment was conducted in a growth chamber at 25 °C, with a relative humidity of 38 80% and a 16 h/8 h light-dark cycle (600 lux light intensity) for 30 days. Sterile ultrapure 39 deionized water was used as the negative control, uncapped and oleic acid (OA) capped SPIONs 40 were also tested to assess their potential effects. Magnetic nanostructures were synthesized by 41 coprecipitation method and characterized by scanning and transmission electron microscopy 42 (SEM and TEM), X-ray diffraction (XRD), Fourier-transform infrared spectroscopy (FTIR), 43 zeta potential, hydrodynamic diameter, magnetic behavior, and release kinetics of chemical 44 cargo. Uncapped and OA-capped SPIONs did not significantly affect soil microbial 45 community. Our results showed an impairment in the soil microbial community exposed to free 46 UA, leading to a general decrease in negative effects on soil-based parameters when bioactive 47 was loaded into the nanoscale magnetic carrier. Besides, compared to control, the free UA 48 caused a significant decrease in microbial biomass C (39 %), on the activity of acid protease 49 (59 %), and acid phosphatase (23 %) enzymes, respectively. Free UA also reduced eukaryotic 50 18S rRNA gene abundance, suggesting a major impact on fungi. Our findings indicate that 51 SPIONs as bioherbicide nanocarriers can reduce the negative impacts on soil. Therefore, nano-52 enabled biocides may improve agricultural productivity, which is important for food security 53 due to the need of increasing food production. 54 Keywords: Nanobiopesticide, Soil microbiology, Usnic acid, Enzymatic activity, Toxicity, 55

56

Safe-by-Design, Nano-Enabled Products

1. INTRODUCTION

The global population is predicted to reach close to 9.1 billion in 2050, necessitating an increase in food production of approximately 70%. ¹ The use of pesticides plays an important role in agriculture by controlling crop pests and, consequently, their use have increased along with the rise in global demand for food. Nevertheless, an indiscriminate growth in the use pesticides has been linked to environment and human health risks. Thus, a technological revolution in agriculture is needed to expand crop production in an environmentally safe way. The development of efficient, precise, and sustainable pesticide formulations to minimize hazardous residues is essential to ensure food safety and environmental security. ² In this scenario, nano-enabled products have attracted great attention in the last decades due to their enhanced performance in agricultural applications, maintaining the action, improving the effectiveness, and controlling the release of pesticide active ingredients. ^{3–5} The current development of nano-enabled agrochemicals with a focus on decreasing the environmental footprint of agriculture has been shown in literature. ^{6,7} Nonetheless, the development of safe-by-design nanoformulations using natural products (biocides) as active ingredients capable to replace commercial agrochemicals and increase food security is still scarce.

Pesticide nanocarriers are expected to grow rapidly in the coming years. ^{8,9} However, the use of nano-enabled agrochemical products will inevitably release them into the environment, which can potentially impact non-target organisms. ^{10–12} The discovery and development of nano-enabled products depend heavily on studies about the effects of nanoformulations, such as nanopesticides and nanobiopesticides, on agricultural soils. Understanding the environmental fate and behavior of nano-enabled products in soil systems is required to promote the development of safe-by-design nanopesticides. A common drawback of conventional synthetic pesticide applications is their lower efficiency and higher environmental losses. ¹³ Therefore, it is highly desirable in pest management systems to deliver

Pesticides to the exact target site and accurate cargo release without losing effectiveness. ¹⁴ Nano-enabled herbicides provide enhanced biocidal performance against weeds compared to active ingredients. ^{3,15} Nevertheless, there are still concerns about their use, which may be harmful to living organisms such as soil microbial communities. ¹⁶ For instance, polymeric nanopesticide damage the activity of acid phosphatase in soil, ¹⁷ and also change the rhizosphere bacterial communities. ¹⁸ The effects of azoxystrobin-loaded silica nanoparticles have been studied, revealing a lower impact on soil microbiota. ¹⁹ The authors demonstrated that nanopesticide formulation was less phytotoxic for *Solanum lycopersicum* plants, even presenting a pesticide uptake of 10-fold higher than the conventional pesticide. ¹⁹ Among these, biopesticides have emerged as attractive alternatives to synthetic agrochemicals. Despite the growing interest on the impact of nanopesticides on soil ^{20,21}, there is still a lack of knowledge on the harmful potential of nanobiopesticides or natural pesticides based-nanoformulations on the soil environment.

Biological systems are natural sources of several active compounds with pesticidal activities. For instance, secondary metabolites could be used as natural pesticides, ²² especially due to high biodegradability, which impedes their accumulation in the environment. Usnic acid (UA) [2,6-diacetyl-7,9-dihydroxy-8-9b-dimethyl-1,3 (2H, 9b/aH)-dibenzofurandione; C₁₈H₁₆O₇] is considered a research priority of this area because of its abundance in diverse lichen species and promising herbicidal properties. UA inhibits chlorophylls and carotenoids biosynthesis *via* inhibition of 4-hydroxyphenyl pyruvate dioxygenase, ²³ promotes the photodegradation of chlorophylls, ²⁴ and inhibits PSII electron transfer at the quinone B (Q_B) catalytic domain. ²⁵ Similar effects on the Q_B domain have been reported for commercial herbicides such as atrazine, diuron, linuron, and others. ^{4,26,27} Additionally, UA is a promising compound to be loaded into a nanocarrier to development of nano-enabled products for sustainable weed control.

Due to the enhanced performance of nano-enabled materials, there is a growing interest in the development of engineered nanosystems, aiming to deliver a variety of active compounds to enhance crop productivity. Literature reports that nanopesticides are around c.a. 31.5% more effective than their conventional analogues (free pesticides). ²⁸ In addition, nanoscale formulations can be used as a strategy to improve the fate, mobility, sorption, and degradation of an active ingredient in the environment. ²⁰ Several studies using organic and inorganic nanomaterials as nanocarriers have been indicating that they may be potentially safer for nontarget organisms. ^{20,29,30} Nonetheless, gaps on the fate of nanobiopesticides in the environment indicate the need for further investigations. Superparamagnetic iron oxide nanoparticles (SPIONs) have been developed and applied for delivery applications as carrier systems. ³¹ To best of our knowledge, the application of SPIONs as nanocarriers for biopesticide delivery has not yet been reported. Moreover, the SPIONs can release chemical cargo in agricultural systems mainly due to their lower toxicity. ³² Also, SPIONs can provide several benefits for agriculture. For instance, they can direct deliver the active compound to target sites in cellular organelles, can be removed from the environment via magnetic collectability behavior, and also could serve as a "trigger" for smart cargo release by magnetic induction application. 33 Magnetic nanostructures are attractive for nanorobotic manipulation, cargo transport, drug/pesticide diffusion, and attachment removal. ^{34,35} Finally, it is also important to point out that the use of SPIONs is also based on their scalable production by different synthesis routes. ^{36,37} For instance, Hammed et al. 37 demonstrated that SPIONs can be scalable produced using a tubular electrochemical system, which they obtained a yield of production of 8.3 mg mol⁻¹ Fe and a productivity of 163 µg mol⁻¹ Fe min⁻¹.

108

109

110

111

112

113

114

115

116

117

118

119

120

121

122

123

124

125

126

127

128

129

130

131

132

In this study, the potential impacts and the fate of SPIONs and oleic acid capped SPIONs (SPIONs@OA) were designed using a simple co-precipitation method as a nanoplatform to carry usnic acid as bioherbicide (SPIONs:UA and SPIONs:UA@OA). The obtained

nanostructures were characterized roundly, and the fate on soil microbial community were investigated in detail. These aspects could be key to the further development and implementation of nano-enabled sustainable and precision agricultural strategies.

136

137

138

139

140

141

142

143

144

145

146

147

148

149

150

151

152

153

154

155

156

157

133

134

135

RESULTS AND DISCUSSION

Characterization of nanocomposite. The SEM (Figures 1b-e) and TEM (Figures 1f-i) micrographs of SPIONs, SPIONs@OA, SPIONs:UA, and SPIONs@OA:UA showed a mean particle size of c.a. 5.21 ± 0.13 , 7.80 ± 0.20 nm, 5.63 ± 0.16 nm, and 7.38 ± 0.25 nm, respectively. These results suggest that two different particle size regimes were observed depending on the presence of OA as a capping agent. SPIONs and SPIONs:UA presented a smaller particle size when compared with SPIONs@OA and SPIONs@OA:UA. The TEM micrographs reveal a slight hint of aggregation of the individual SPIONs coated with oleic acid. Additionally, the unimodal behavior of particle size distribution was observed in the TEM micrograph. Similar particle size was also observed by Forini et al. 26 using SPIONs@OA to induce magnetic collectability in microparticles as a delivery system for atrazine. On the other hand, SEM images reveal a trend to the aggregation of particles; these results are confirmed by hydrodynamic diameter analysis (Figure S1). However, SPIONs, SPIONs@OA, SPIONs:UA, and SPIONs@OA UA showed PDI values around c.a. 0.515, 0.387, 0.293, and 0.406, respectively (Figure S1 in the Supporting Information).). Zeta potential (ZP) is a physical property of nanostructures that controls electrostatic interactions in particle dispersions and is an essential property to understanding the stability of colloidal dispersion. ³⁸ The ZP of SPIONs, SPIONs@OA, SPIONs:UA, and SPIONs:UA@OA is highly influenced by pH (Figure S2 in the Supporting Information).); positive surface charges are presented at low pH and negative at high pH. The isoelectric point for SPIONs, SPIONs, SPIONs@OA, SPIONs:UA, and SPIONs: UA@OA is 4.31 ± 0.05 , 4.79 ± 0.03 , 5.35 ± 0.01 , and 8.91 ± 0.05 , respectively (**Figure** **S2** in the Supporting Information). Additionally, the magnetization curves as function of the applied magnetic field have not shown any hysteresis, i.e., zero coercivity, corroborating that the samples are in a superparamagnetic state at room temperature (**Figure S3** in the Supporting Information). This magnetic behavior is essential for environmental applications since the particles will only be magnetized in the presence of an external magnetic field. ³⁹



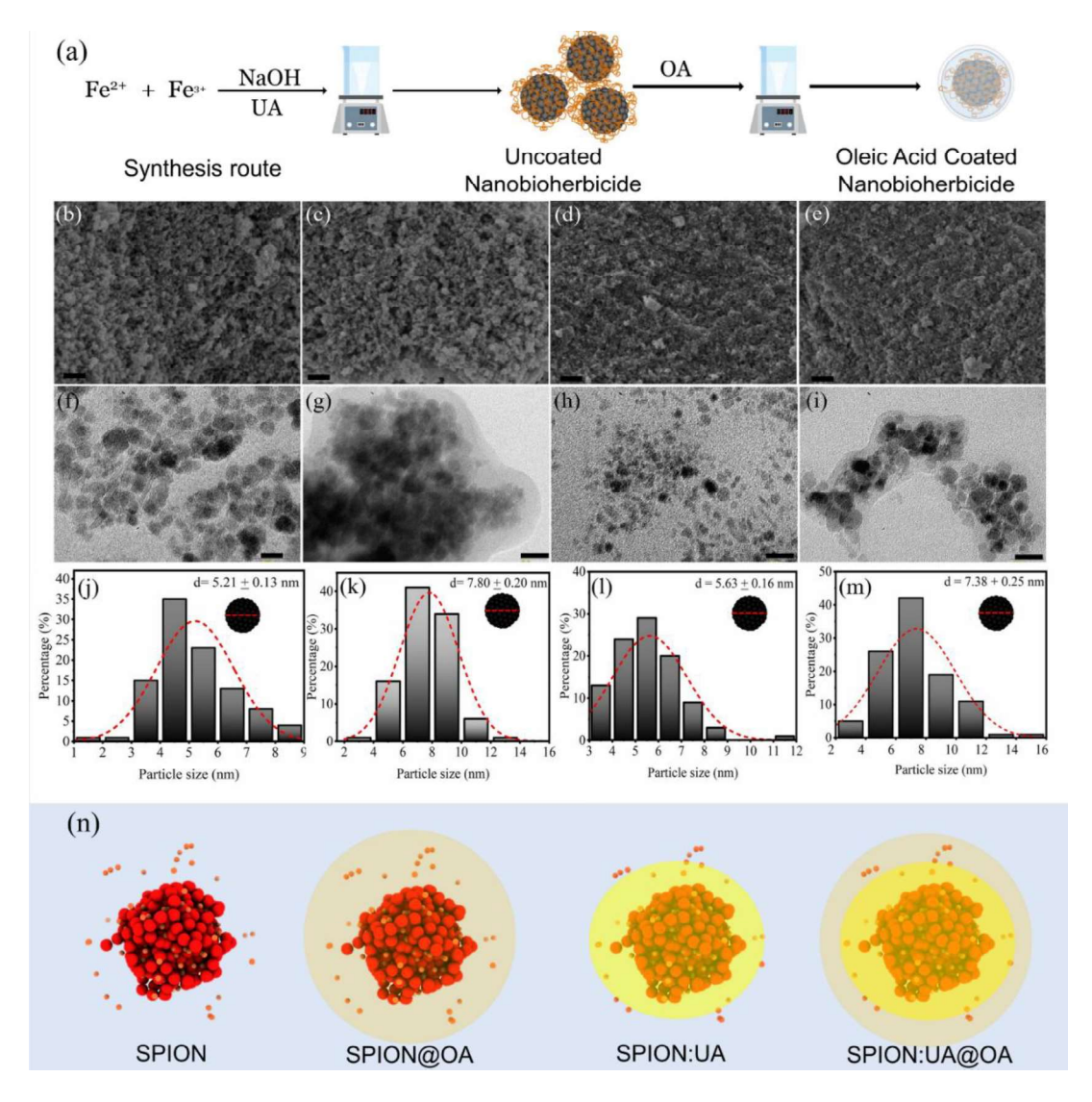


Figure 1. Characterization of the nanocomposite samples: (a) Schematic representation of synthesis of the uncoated and oleic acid-coated nanoarchitectured system; SEM images of the (b) SPIONs, (c) SPIONs@OA, (d) SPIONs:UA, and (e) SPIONs:UA@OA; TEM images of the (f) SPIONs, (g) SPIONs@OA, (h) SPIONs:UA, and (i) SPIONs:UA@OA; and (j-m) their respective size distribution histograms. (n) schematic representation of SPIONs, SPIONs@OA, SPIONs:UA, and SPIONs@OA:UA. Scale bar: (b-e) 100 nm and (f-i) 20 nm. n=100.

Fourier-transform infrared (FTIR) spectra demonstrated that the characteristic peaks of the UA fingerprint region (c.a. 1750 - 876 cm⁻¹) could be observed for SPIONs:UA and SPIONs@OA:UA (Figures 2a,b). The characteristic IR absorption peaks of UA are observed, for instance, at 1630 cm⁻¹ (the stretching vibration mode of the O-H bond), due to the intramolecular hydrogen bond, thus confirming the presence of UA on the magnetic nanoparticle (Figure 2b). 40,41 The acid-base complex formation between NaOH and OA during SPIONs@OA synthesis suggests that deprotonated OA can easily be adsorbed by the SPIONs surface. This insight was previously observed via molecular mechanics and dynamics modeling. ⁴² The infrared absorption peak at $c.a. \sim 1280 \text{ cm}^{-1}$ can be observed for SPIONs@OA and SPIONs:UA@OA reveals the -C-OH stretching vibration mode of OA. 43 The OA also showed the C-H stretching vibration modes observed at 2922 and 2860 cm⁻¹. The infraredspecific absorption peaks of Fe-O bonding are regarded at $c.a. \sim 570$ and 549 cm^{-1} . ⁴⁴ In **Figure** 2c, a vibrational peak at 1632 cm⁻¹ can be observed that has been shifted to 1710 cm⁻¹, related to C=O bending symmetric vibration in oleic acid due to the deprotonation of the -COOH group. ⁴⁵ These results suggest that OA performs hydrogen bond formation via their carboxyl group with oxygen atoms of the hydrophobic usnic acid molecule (carbonyl and/or furan groups, respectively). The -COOH groups of oleic acid when associated with Fe atoms, which render a partial single-bond behavior of the C=O bond to weaken the bond and, consequently, shift the stretching frequency to a lower value. ⁴⁶ Literature reports usnic acid as a Fe²⁺ chelating agent, capable of capturing Fe²⁺ ions as a metal-binding agent. ⁴⁷ Additionally, DFT reactivity descriptors calculations were applied to discuss the UA interactions with Fe²⁺ (see **Table S1** and Figure S4 in the Support Information for details). Due to the addition of UA before nanostructure synthesis, the UA may be linked during the co-precipitation with Fe₂⁺ ions, consequently attached to the nanoparticle structure.

172

173

174

175

176

177

178

179

180

181

182

183

184

185

186

187

188

189

190

191

192

193

194

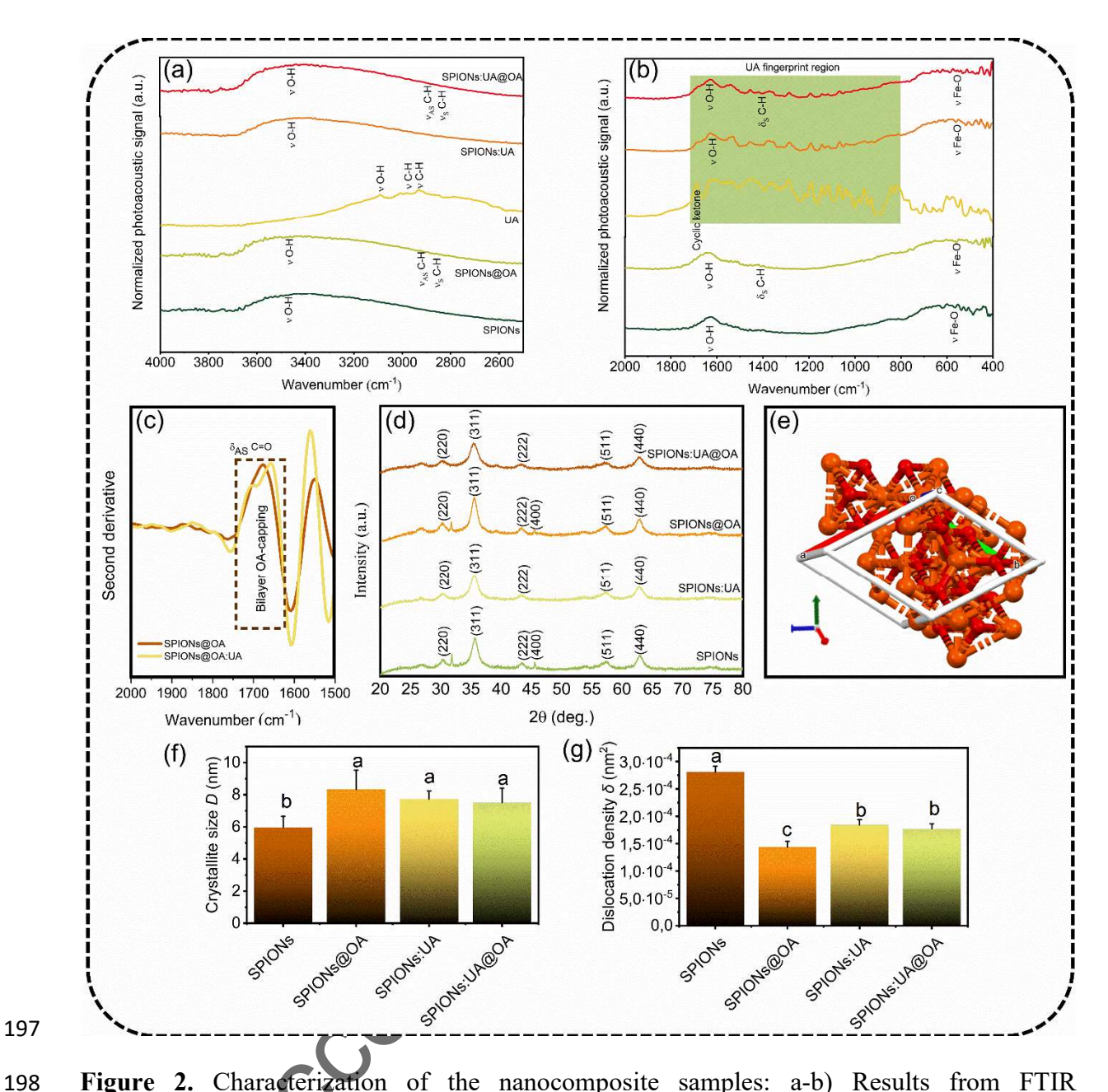


Figure 2. Characterization of the nanocomposite samples: a-b) Results from FTIR spectroscopy; c) second derivative of FTIR spectroscopy; d) X-ray diffraction patterns; e) crystallographic structure, f) crystallite size, and g) dislocation density behavior of SPIONs, SPIONs@OA, SPIONSs:UA, and SPIONs:UA@OA. Significant differences are indicated by different letters shown above the error bars (p < 0.05).

197

199

200

201

202 203

204

205

206

207

208

The X-ray diffraction (XRD) analysis results of our nanocomposite are shown in Figure 2d. Our data also confirmed the single-phase crystal formation, in which all the reflection peaks were identified according to the crystallographic structure of a magnetite pattern. ³¹ The observed XRD powder diffraction was in good agreement with the Crystallographic Open Database (COD 96-900-2318). The diffraction pattern of the product was (220), (311), (222), (400), (511), and (440). The average crystallite sizes were calculated by using the Scherrer equation as D = 5.96 nm, 7.73 nm, 8.33 nm, and 7.51 nm, for SPIONs, SPIONs@OA, SPION:UA, and SPION@OA:UA, respectively (Figure 2f). In general, the TEM results agreed with those of XRD measurements for narrow grain-size distributions. On the other hand, SPIONs:UA exhibited large particle sizes in XRD compared with TEM values. It is important to note that the TEM measures the particles' diameter size, including the nucleus and cover generated during synthesis, ⁴⁸ whereas XRD measures the SPIONs' crystallite size. ⁴⁹ The observed values for dislocation density (in nm²) are also shown in Figure 2g, indicating that the presence of OA and UA on SPIONs reduced dislocation density in the nanocomposites, most likely due to the association of UA and OA molecules on the SPION structure. Also, according to Rietveld refinement, the crystallite structure of SPIONs presents a cubic diffraction plane (Figure 2e).

Release kinetics. The *in vitro* release kinetics of UA were studied by fitting the cumulative release data (Figure 3a,e). The release of UA from SPIONs:UA was evaluated and the time for nanostructures releasing 50% of the UA release (t50%) was *c.a.* 859 minutes (Figure 3b). The release profile of UA from SPIONs:UA@OA showed that *c.a.* 1086 minutes was the t50% (Figure 3f). Several mathematical models have been used to interpret the chemical cargo release kinetics data with their associated release mechanisms. ⁵⁰ Thus, the best four different mathematical models such as Zero order, Hill, Weibull, and Korsmeyer-Peppas were used to fit the experimental released profile of UA. The model which fitted best with the release profile data was identified by a high correlation coefficient (R²). In both cases, the release profile of UA from SPIONs:UA and SPION@OA:UA nanocomposites have shown the best fits with Weibull's and Korsmeyer-Peppas' equations (Figure 3cd and Figure 3gh). The SPIONs:UA and SPION@OA:UA presented a R² values of 0.999 in both cases Weibull's and Korsmeyer-

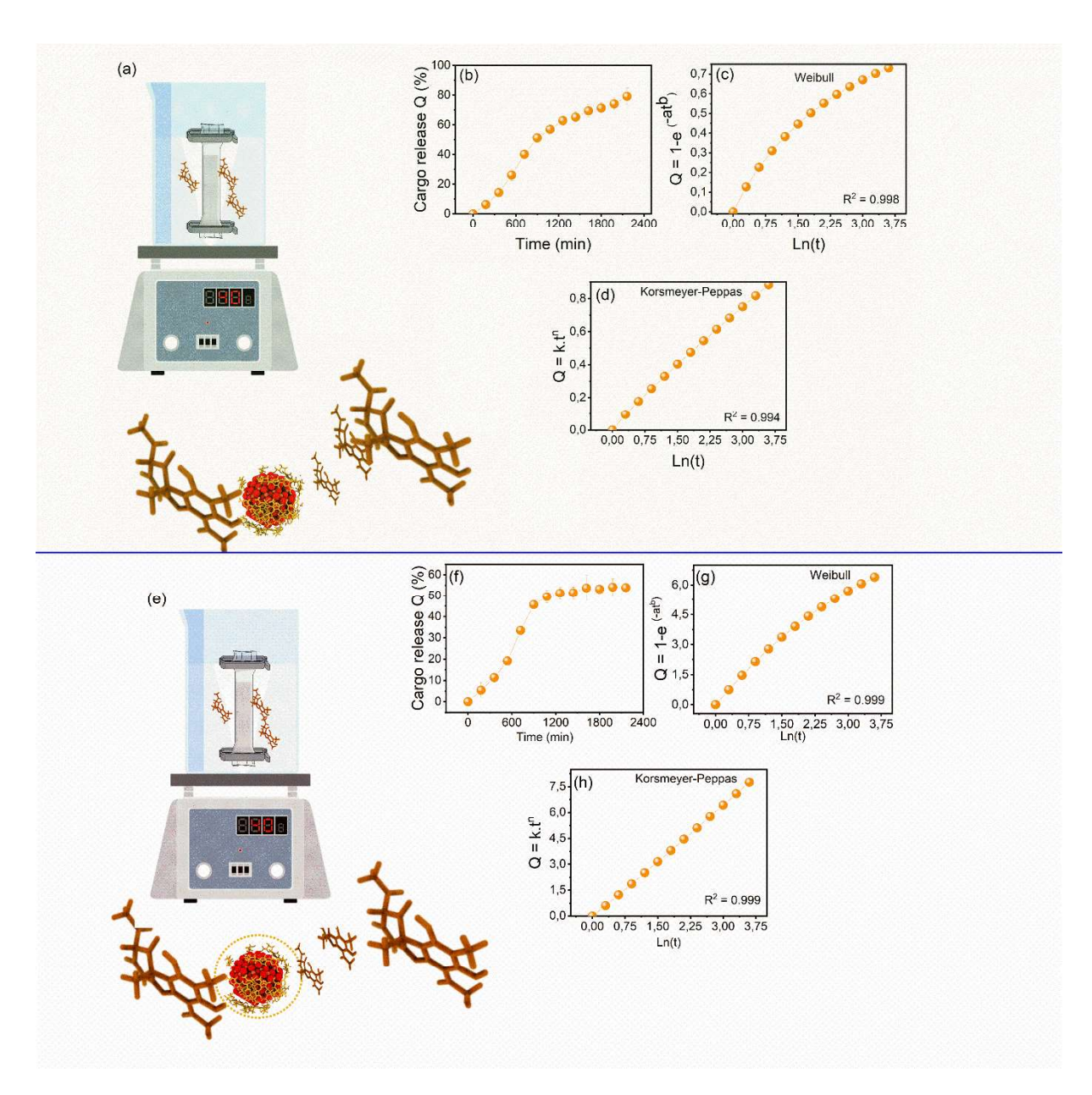


Figure 3. (a) Schematic illustration of *in vitro* cumulative cargo release kinetics of usnic acid from SPIONs:UA in deionized water (25 °C) donor and the other an acceptor compartments of assay, (b) cumulative release kinetics of usnic acid from SPIONs:UA, (c) Weibull mathematical model obtained from the cumulative cargo release kinetics curve of usnic acid from SPIONs:UA, and (d) Korsmeyer-Peppas mathematical model obtained from the cumulative cargo release kinetics curve acid from SPIONs:UA, (e) Schematic illustration of *in vitro* cumulative cargo release kinetics of usnic acid from SPIONs:UA@OA in deionized water (25 °C) donor and the other an acceptor compartments of assay, (f) cumulative release kinetics of usnic acid from SPIONs:UA@OA, (g) Weibull mathematical model obtained from the cumulative cargo release kinetics curve of usnic acid from SPIONs:UA@OA, and (h)

Korsmeyer-Peppas mathematical model obtained from the cumulative cargo release kinetics curve acid from SPIONs:UA@OA. (n = 5).

The *b* values of the Weibull function (b = -6.7251 and -6.9928) were observed for SPIONs:UA and SPIONs:UA@OA, respectively, when b > 1 suggests that complex mechanisms govern the release process of UA in both nanostructures. The Weibull dissolution constant rate (K_W) observed were 833.12 min^{-0.5} and 1088.76 min^{-0.5}. The *n* value (Korsmeyer-Peppas model) observed was 0.896 ± 0.006 for SPIONs:UA, and 0.888 ± 0.007 for SPIONs:UA@OA, when the values of *n* were greater than 0.5 but less than 1.0, suggesting that release occurred via anomalous diffusion in both forms of nano-enabled usric acid. ⁵¹ The value of dissolution efficiency (DE) was 42.12 % and 37.94 % for SPIONs:UA and SPIONs:UA@OA, and the mean dissolution time (MDT) values computed were 847.69 and 639.58 minutes, respectively.

Soil microbial community activity. Soil microbial biomass C was significantly affected by magnetic nanoparticles treatments. Smaller values of microbial biomass C were observed for UA and SPIONs:UA treatments, reducing around 38% and 14% of the microbial biomass, respectively, when compared with control soil. In contrast, microbial biomass for SPIONs@OA and SPIONs:UA@OA treatments was not significantly different from that of control samples (Figure 4a). In general, the microbial biomass trend to decrease steadily with magnetic nanoparticles-carrying UA, whereas the addition of uncoated SPIONs significantly increased the microbial biomass in the soil, suggesting a potential consumption by microorganisms of Fe ions released from uncoated SPIONs. ⁵²

Notably, the enzymatic activities of the soil microbial community were also affected by magnetic nanocarrier treatments. The activity of β -glucosidase showed in **Figure 4b**, presented maximum values for control and SPIONs@OA treated soils, respectively. All other treatments

lead to a decrease in \(\beta\)-glucosidase activity and give rise to a more pronounced decrease in activity in the presence of UA and SPIONs:UA@OA. Additionally, β -glucosidases are expressed by a wide range of microorganisms and are composed of a heterogeneous group of phylogenetically conserved and hydrolytic enzymes (plant biomass). ⁵³ The interaction between soil and nano-enabled products may result in altered microorganism-driven biochemical processes. 16,54–56 In the current study, the results of acid protease activity revealed that there UA, SPIONS:UA and SPIONs:UA@OA was decreased, equal to approximately ~55% decrease with UA treatment and ~45% for SPIONs:UA, respectively (Figure 4c). These findings indicate that UA can act as a biocide in soil, especially in the fungal community. The enzyme is responsible for hydrolyzing proteins into amino acids, thereby promoting fungal growth in soil. 57 Further evaluation of acid phosphatase activity showed that only UA significantly inhibits their activity (Figure 4d). These findings also indicate that the SPIONs:UA and SPIONs:UA@OA may decrease cargo toxicity on non-target organisms. Acid phosphatase in soil microorganisms plays an important role in transforming phosphorus (P) compounds into a species that can be directly utilized by plants. 56,58 The decreased toxicity behavior of our nano-enabled bioherbicide on soil microorganisms is similar to a series of nanopesticides previously studied compared to conventional pesticides. 16,59 A schematic procedure of soil samples studied and nanoparticles are presented in Figure 4e.

274

275

276

277

278

279

280

281

282

283

284

285

286

287

288

289

290

291

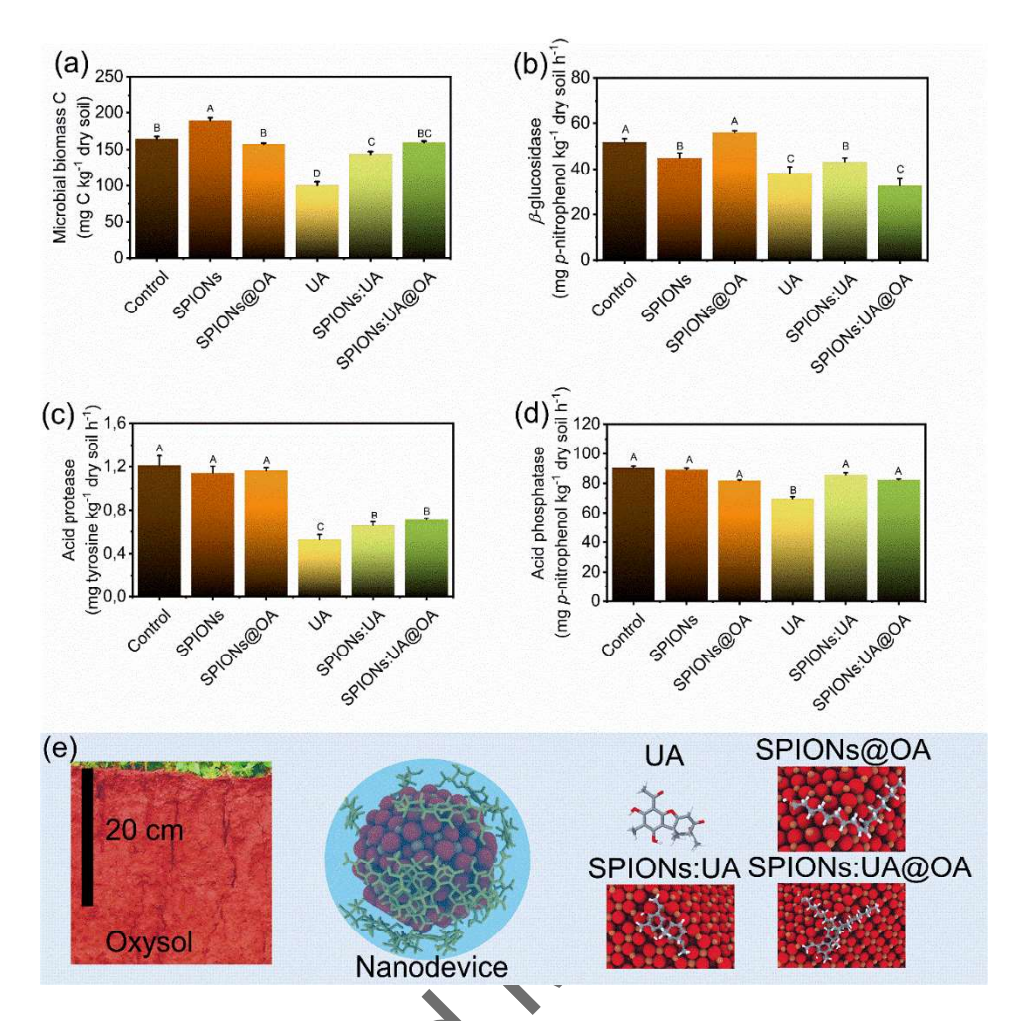


Figure 4. (a) Soil microbial biomass. Enzymatic activity of (b) β -glucosidase, (c) acid protease, and (d) acid phosphatase in a dystrophic red latosol soil spiked with SPIONs, SPIONs@OA, usnic acid, SPIONs:UA, and SPIONs UA@OA at 500 ppm, dry soil and incubated for 30 days. (e) schematic illustration of soil sample and treatments. Values are medians \pm standard error (n = 3), and different letters indicate the statistical difference at the p < 0.05 level by Kruskal Wallis test.

Soil microbial community maintenance depends on their homeostatic ability to face the complexity of exogenous environmental changes and disturbances, ^{60,61} such as nano-enabled pesticides and biopesticides. ^{18,62} The effect of these materials on soil microbiota can be evaluated by the strength of connectivity among elements interacting in a biological network such as the approach proposed by Amzallag. ^{63,64} A systemic approach was used to evaluate the global connectance of the soil microbial community (Cg_{Total}). The Cg_{Total} results revealed a decline in the stability of the microbial community, as can be seen, by the reduction in connection strength among the evaluated parameters (**Figure 5**). **Figures 5a–f** displays the

Pearson's correlation coefficients (r) between each paired variable investigated in the systemic network. Our results revealed differences in the strength of the relationships between paired variables as shown in the correlogram plots (Fig. 5a–f), confirming that the bioherbicide and their nanoformulation changed the modulation of microbial community functioning. 60

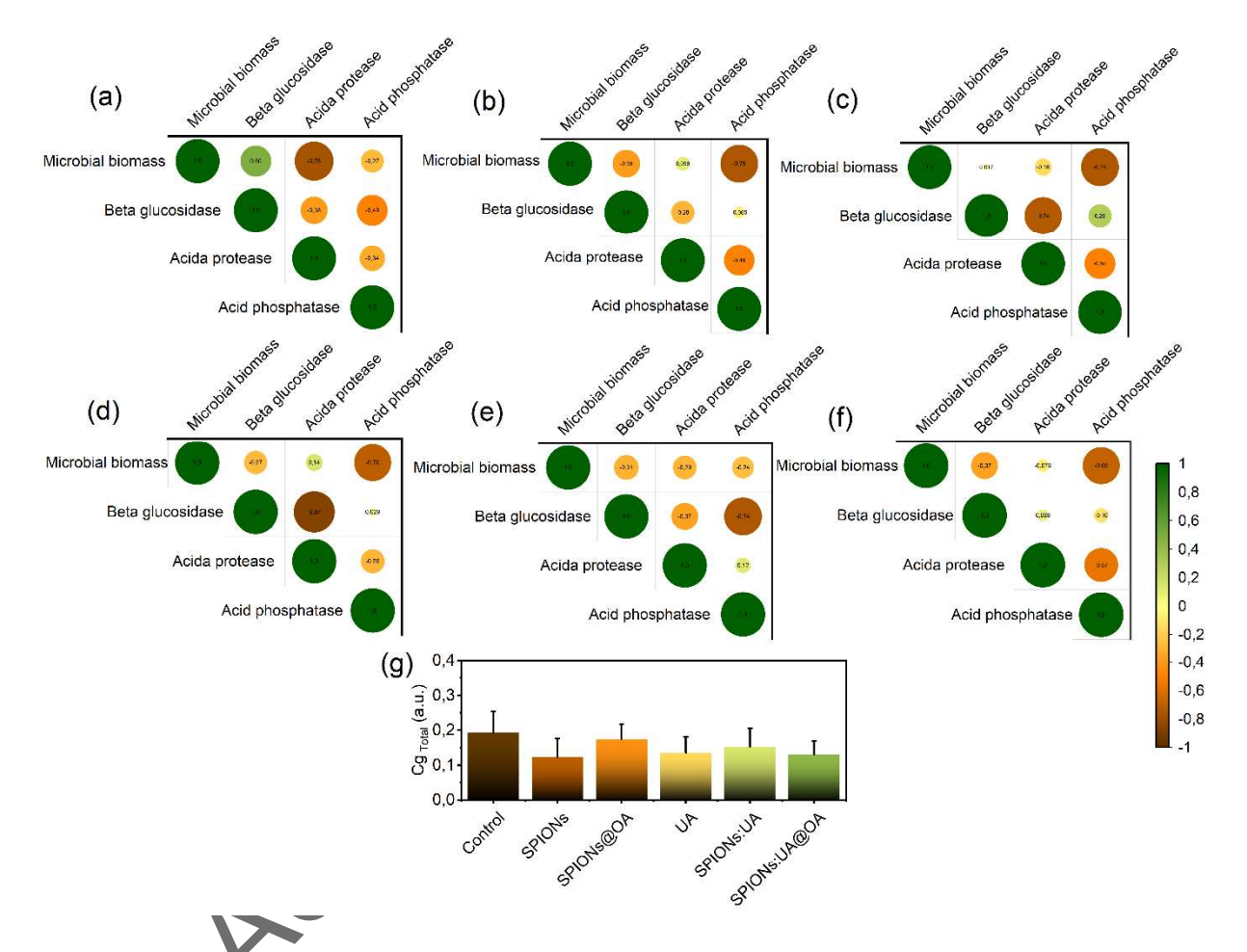


Figure 5. A correlogram depicting the Pearson's correlation coefficients of soil microbial community activity (microbial biomass and enzyme activity), (a) control – untreated soil, (b) SPIONs, (c) SPIONs@OA, (d) usnic acid (UA), (e) SPIONs:UA, and (f) SPIONs:UA@OA treated soil. (g) Global network connectance values observed in this study.

According to global connectance values, considerable modifications were observed in the system's network mainly for SPIONs, UA-treated soil and SPIONs:UA@OA carrying bioherbicide (**Figure 5g**). Biological systems show emergent properties (*i.e.*, nonlinear interactions among the network of their components) that define their adjusted state to regular

environmental conditions and evidence their destabilization under environmental stressors, ⁶⁵ modeling the complexity of living systems. ⁶⁶ Our data showed some differences among treatments concerning how the microbial community adjusts their function to imposed soil treatments. Consequently, it corroborates the idea that nano-enabled agrochemicals affect the homeostatic dimension of living systems, such as the integration and organization of their parts in a network. ⁶⁶ Our data showed a decrease in the connectance of microbiome network values with the exposure of usnic acid, which is related to the homeostatic maintenance of microbial fitness. On the other hand, SPIONs@OA and SPIONs:UA showed a general increasing in the *Cg_{Total}*, suggesting a higher modulation (homeostatic adjustment) of soil microbiota. According to Bertolli *et al.*, ⁶⁷ this increased connectance value indicates great system stability, up to a critical threshold. Additionally, further studies and more effort, are needed to understand the effects of nano-enabled pesticides on the homeostatic dimension level in biological systems.

Quantitative analysis of soil bacterial and eukaryotic abundance by qPCR. Our experiment found high amplification efficiency (96.2% to 107%) in PCR samples, with a high consistency (R² = 0.981–0.989). The abundance of the soil bacterial and eukaryotic community, based on the 16S and 18S rRNA number copy and their changes under UA, SPIONs:UA, and SPIONs:UA@OA exposure as well as the untreated soil sample used as control, are presented in Figure 6. Although the soil bacterial community showed susceptibility to UA and all tested nanoformulations tested (Figure 6a), our results suggest a strong decrease in the abundance of the soil bacterial and eukaryotic communities when the soil was treated with UA (Figure 6a,b). On the other hand, the soil bacterial community did not show any significant differences compared with nanocomposites carrying UA (SPIONs:UA and SPIONs:UA@OA). UA has been shown to have greater antibacterial and antifungal activity. ^{68,69} According to Maciag-Dorszynska *et al.*, ⁷⁰ the main routes of UA's antimicrobial action are probably related to the

inhibition of RNA synthesis and elongation of DNA replication. The evidence that ionic UA and UA-loaded nanocomposites reduce the abundance of 16S rRNA gene copies related to the bacterial community compared to untreated soil samples highlights the risks to these groups of soil microbiota. For 18S rRNA gene copies related to the eukaryotic community, UA and SPIONs:UA@OA presented a major impact on the eukaryotic community abundance. These results reinforce our previous findings on acid protease results showing that the fungal community was less tolerant to UA and SPIONs:UA@OA. Furthermore, our findings show a direct relationship between the toxic behavior and the potential fate of the SPIONs-framework on soil microbial communities as observed for Cu(OH)₂-based nanopesticides. ⁷¹ Additionally, our general results suggest that the sustained release of UA from the SPIONs-framework may be a key factor in minimizing the harmful impact of UA on soil microbiota as illustrated in CCE SIEO INIO Figure 6, especially on the fungal community.

349

350

351

352

353

354

355

356

357

358

359

360

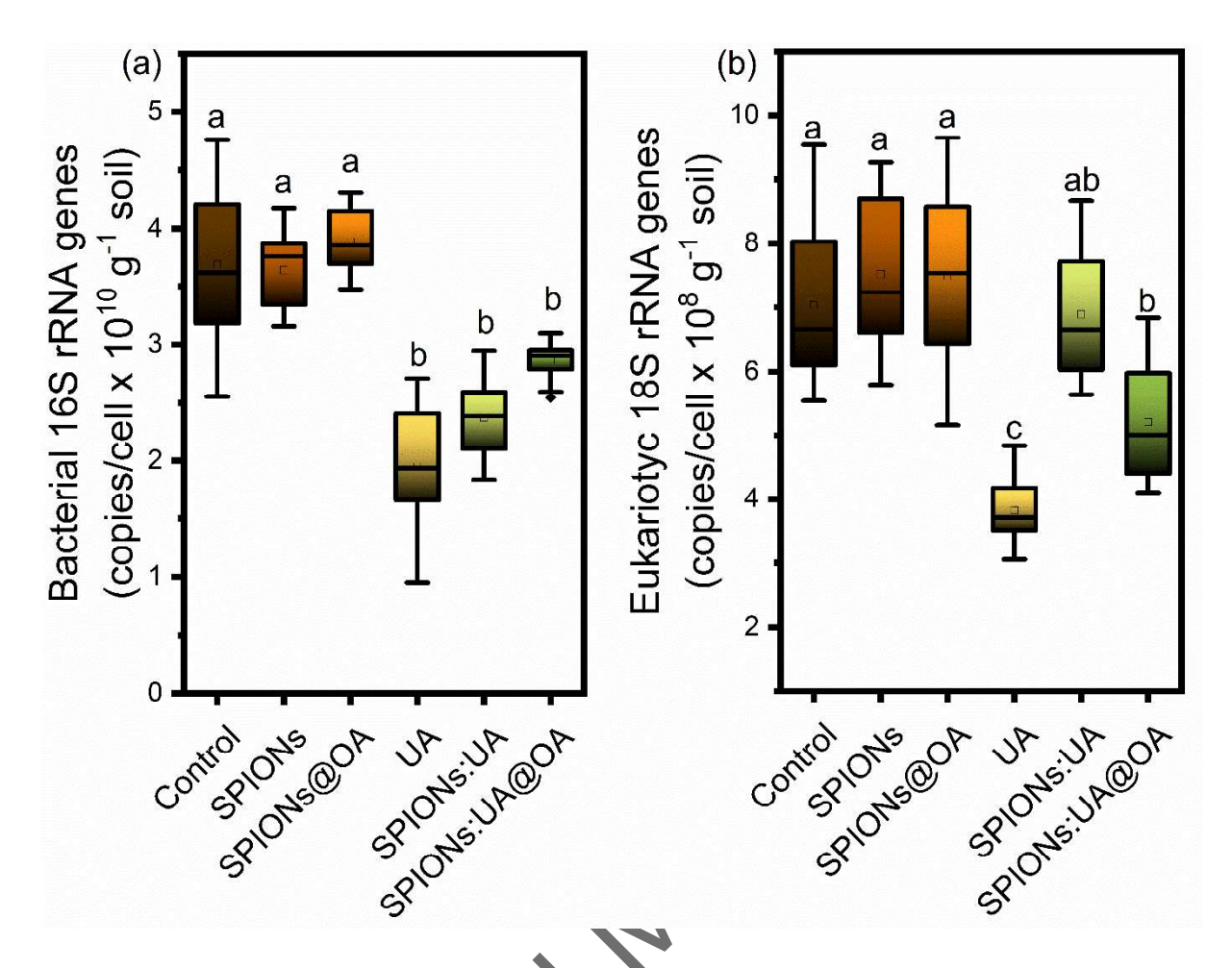


Figure 6. Shifts in copy numbers of (A) bacterial 16S rRNA genes and (B) eukaryotic 18S rRNA genes in response to UA, and SPIONs-framework carrying UA. Data are expressed as the means with standard deviation (SD). Significant differences are indicated by different letters shown above the error bars (P < 0.05) and mean separation was assessed by Student t test.

Additionally, the free UA and carried as SPIONs:UA and SPIONs:UA@OA showed herbicidal activity in both forms, the fully inhibition of PSII electron transport were observed within 72 h as shown in Supporting Information. Figure S10 shows the chlorophyll fluorescence data, these results reveal that nano-enabled usnic acid are more effective than equivalent free UA at similar dose to inhibit PSII. Our result strongly corroborates with the efficiency of nanostructured UA when compared with free UA, by the inhibition of PSII electron transport flux from QA to QB (herbicide-D1 binding niche). A number of strategies have been proposed to control and manage agricultural pests in the last decades. ⁷² Nowadays, nanotechnology has been notable development of nanomaterials and nano-enabled products to agri-food sector due

to increased food demand. The nanopesticides based on biomaterials are promising, 4 and representing a direction for sustainable agriculture development, a safe-by-design strategy to ensure successful scalability, and able to increase food production. ^{73,74} However, at the long term, replacing conventional pesticides seems far from reality, since several nanoformulations present difficulties in scaling up, and little is known about the mechanisms of action and impact against non-target organisms, 72 which difficult its regulatory aspects and consequently a good consumer perception. However, according to IUPAC, 75 nano-enabled pesticides were named as one of ten "chemical innovations" that will change the world in a sustainable way. 76 Therefore, further studies are needed since changes induced on non-target organisms may play a key role in its environmental fate. Thus, our findings contribute to a better understanding of the impact of nanobiopesticides, indicating a possible way to create a more environmentally safe agricultural pest management. Our strategy also indicates a "from nature-to-nature" effort, ideal for a circular bioeconomy landscape. Additionally, nanobiopesticides may be more costeffective and safer than traditional agrochemicals, and also can be an important part of the emerging concept of circular bioeconomy, as they can provide a wide range of benefits, from improved efficiency to enhanced biodegradability. 77,78

393

394

395

396

397

398

399

400

401

392

377

378

379

380

381

382

383

384

385

386

387

388

389

390

391

CONCLUSION

The results reported in this work provide important information concerning the use of nanostructured systems with usnic acid. Usnic acid-loaded SPIONs demonstrate good physicochemical properties, effectively stable lower sizes, possess well-defined structural features, and release over time governed by diffusion processes. These excellent properties allow for its potential agricultural application. In the present study, the soil microbial community impact of uncoated and oleic acid-coated AU-loaded SPIONs was investigated in a dystrophic red latosol (oxysol). In both exposure treatments (UA, SPIONs:UA, and

SPIONs:UA@OA), nano-enabled usnic acid showed less toxicity than the soluble usnic acid compound. These results suggest that the gradual release of UA from nanostructures may affect the toxicity behavior on soil microbiota. The enzymatic activity of acid protease and acid phosphatase was significantly affected by soluble UA. Additionally, the PCR results showed that eukaryotic 18S rRNA genes are affected by UA, suggesting a major susceptibility of the fungi community to UA and SPIONs:UA@OA. Global network connectance analysis suggests that SPIONs are able to modulate the homeostatic behavior of UA on soil microbiota, especially uncoated UA-loaded SPIONs. In summary, our present findings suggest that SPIONs as nanocarriers can potentially reduce the environmental impact of biopesticides on the soil an list microbiota.

412

413

414

415

416

417

418

419

420

421

422

423

424

425

426

402

403

404

405

406

407

408

409

410

411

EXPERIMENTAL PROCEDURE

Synthesis and characterization of SPIONS: UA@OA. SPIONs were prepared by the coprecipitation method using iron salts in an alkaline medium. ^{26,31} FeCl₃.6H₂O (7.4 x 10⁻⁴ mol L⁻¹) and FeCl₂.4H₂O (1.7 x 10⁻³ mo L⁻¹) were solubilized in 200 mL of the aqueous medium, then 8 mL of sodium hydroxide (NaOH 9.46875 mol) with and without 500 mg of UA (1.4 x 10⁻³ mol) were added and stirred for 10 minutes at 50 °C. Next, 2.5 mL of oleic acid (OA at 5.3 x 10⁻³ mol) was added, and the mixture was heated at 80 °C for 1 h. Then, consecutive washes with water and ethanol were performed. Finally, the SPIONs, SPIONs:UA, SPIONs@OA, and SPIONs@OA:UA were dried.

morphology and size of SPIONs, SPIONs@OA, SPIONs:UA, SPIONs@OA:UA were determined by scanning electron microscopy with a field emission gun (SEM, JSM-7500F, JEOL), and 200 kV transmission electron microscopy (TEM, CM200, Philips). X-ray diffraction (XRD) patterns were obtained using a Rigaku MiniFlex 600 W Xray diffractometer with Bragg-Brentano geometry and Cu K radiation (1.54056) and a detector HPAD (HyPix-400 MF 2D) (Rigaku Corp, Tokyo, Japan). The average crystallite size (D) and
 dislocation density (δ) values of the SPIONs, SPIONs@OA, SPIONs:UA, and
 SPIONs@OA:UA were estimated from Debye-Scherrer's and Williamson-Hall's equations
 [eq. 01 and eq. 02]:

$$432 D = \frac{K\lambda}{\beta \cos\theta} [eq. 01]$$

$$\delta = \frac{1}{D^2}$$
 [eq. 02]

where, K is the Scherrer constant, λ is the wavelength of X-rays (1.54056 Å), β is the full width at half maximum of the diffraction peak (in radians), and θ is the Bragg angle. ⁷⁹ The δ is the dislocation density value. ⁸⁰

The surface chemical characteristics were studied by a Fourier-transform infrared photoacoustic spectrometer (FTIR-PAS, Thermo Nicolet 6700) in the spectral range from 4000 to 400 cm⁻¹. The zeta potential was measured by analyzing SPIONs, SPIONS@OA, SPIONs:UA, and SPIONs@OA.UA using the Zetasizer Nano ZS (Malvern). Briefly, 0.2 g of nanoparticles were dispersed in 200 mL of 1 mmol/L NaCl solution and sonicated for 10 min at a power setting of 80 W. The pH of the dispersion was adjusted to the desired value in the pH range 2-10 with 0.1 mol/L HCl or NaOH. The dispersion was then allowed to settle for 24 h and the supernatant was used for zeta-potential measurement. **Figure S2** in the Supporting Information displays data.

Release kinetics assay. The release of UA from magnetic nanocarriers was investigated based on a release test using two compartments (one donor and the other acceptor) separated by a dialysis membrane with 10 kDa molecular exclusion pores, using 0.1 g of SPIONs:UA@OA at

room temperature under a magnetic stirrer. ²⁶ The amount of released UA from a certain amount of magnetic nanocarrier was measured according to Chircov *et al.* ⁸¹ by following equation [eq. 03] using a UV-Vis spectrometry:

456
$$Cargo \ release \ (\%) = \frac{M_i}{M_t} \ x \ 100\%$$
 [eq. 03]

where, M_i is the concentration of usnic acid released at time i and M_t is the initial concentration of usnic acid added to the magnetic nanocarrier solution.

The mechanism of release profile of SPIONs:UA@OA was evaluated by Zero-order, First-order, Korsmeyer-Peppas, Weibull, and Hill mathematical models using the software KinetDS. ⁸² Detailed information is presented in **Table S2** and **Figure S5** in Supporting Information.

Soil sampling. For the soil test, a dystrophic red latosol (oxysol) was collected from the top 20 cm of surface soil from an agricultural land located at Rio Brilhante city (Figure S6 at Supporting Information). Mate Grosso do Sul State, Brazil (54°33'28.037" S and 21°46'33.442" W). The soil pH and soil organic matter (SOM) are 5.06 and 7.43%, respectively. The collected soil samples were air dried and sieved through a 2 mm mesh followed by homogenization, and stored in the dark at room temperature until used. The physicochemical characterizations of dystrophic red latosol (oxysol) are presented in Tables S3 and S4 in the Supporting Information. The dystrophic red latosol used was collected without environmental contamination.

Approximately 500 g of dry soil was weighted into each polyethylene container (1000 mL). Ultrapure deionized water was added into the soil to reach a moisture content of 60% of the maximum water holding capacity. Before the application of treatments, the soils were

allowed to equilibrate for 1 week in the laboratory (20 °C, 80% humidity, and 24h dark). Herein, 500 ppm of UA or SPIONs-framework carrying UA were diluted in sterile deionized water to achieve the selected dose and applied by hand sprayer on the top of the soil. The experiment was conducted in a growth chamber at 25 °C, 80% humidity, and a 16 h/8 h light-dark cycle (600 lux light intensity) for 30 days. During the experimental time, the moisture content of the soil samples was maintained at 60% of the maximum water holding capacity by replenishing the weight loss with ultrapure deionized water.

Microbial biomass C. Microbial biomass C was determined in triplicate and is expressed in milligrams C per kilogram of dry soil (mg C kg⁻¹ dry soil). Microbial biomass C was measured using the chloroform fumigation-extraction method. ⁵⁵ First, 10 g of soil samples were weighed and fumigated with ethanol-free chloroform for 24 h at 25°C under dark conditions. Fumigated and non-fumigated samples from each treatment (untreated, UA, SPIONs, SPIONs@OA, SPIONs:UA, and SPIONs:UA@OA) were extracted with 50 mL of 0.5 M K₂SO₄ on a rotary shaker at 300 rpm for 30 min. The soil sample solutions were filtered and stored at -15 °C prior to analysis on a TOC/TN analyzer (Shimadzu Corp., Kyoto, Japan). See details in Figure S7 (in the Supporting Information)

Microbial enzyme activity. The β -glucosidase activity was measured according to Hamidat and co-authors. ⁸³ Fresh soil samples (10 g) were incubated for 1 h at 37 °C with 40 mL of 0.05 M modified universal buffer (pH 6.0) and 10 mL of 25 mM 4-nitrophenyl β-D-glucopyranoside. The reaction was terminated by adding 5 mL of 0.5 M CaCl₂ and 20 mL of 0.1 M trishydroxymethyl. The β-glucosidase activity was determined by absorbance at λ 408 nm in triplicate and expressed as mg of p-nitrophenol kg⁻¹ dry soil within 1 h.

The acid protease activity was determined as described by Ge et al., ⁸⁴ according to a standard procedure using casein as a substrate. Fresh soil samples (200 mg) were incubated for 2 hours at 50 °C with 500 μ L 0.2 M Tris buffer pH 8.0 and 500 μ L of 20 g.L⁻¹ casein solution under agitation with a magnetic stirrer. The reaction solution was stopped by adding 500 μ L of 30% trichloroacetic acid, followed by centrifugation at 5,000 g for 12 min. 100 μ L of supernatant was mixed with 200 μ L of 500 mM Na₂CO₃ and 100 μ L of 3-fold diluted Folin and Ciocalteu's phenol reagent. Then, the mixture was incubated for 1 hour at room temperature, and the absorbance was measured at λ = 700 nm. As a standard, L-tyrosine was used for the calibration curve and the released L-tyrosine concentration was determined. Protease activity is expressed as mg of tyrosine kg⁻¹ dry soil within 1 h.

The acid phosphatase activity was analyzed using p-nitrophenyl phosphate according to the protocol by Tabatabai. ⁸⁵ Five g of air-dried soil were suspended in 1 mL of toluene, 5 mL of p-nitrophenyl phosphate, and 5 mL of modified universal buffer (pH 5.0), and incubated at 37 °C for 24 hours. After incubation, samples were filtered and the absorbance of p-nitrophenol (pNP) was measured at 410 nm. The acid phosphatase activity was expressed as mg of *p*-nitrophenol kg⁻¹ dry soil within 1 h. Standard curves are presented in the Figure S8 and Table S5 (in the Supporting Information).

Real-time quantitative PCR of bacterial 16S rRNA genes and eukaryotic 18S rRNA genes.

The abundance of bacterial 16S rRNA genes (519F and 907R primer set) and eukaryotic 18S rRNA genes (Euk1A and Euk516R primer set) was evaluated as previously described by Feng et al. ⁸⁶ The primers used in this study are presented in Table S6 in the Supporting Information. The abundance quantification of bacterial 16S rRNA and eukaryotic 18S rRNA genes was measured by real-time qPCR using an iTaq Universal SYBR Green PCR master mix equipped with a CFX96Tm real-time PCR detection system (Bio-Rad) for each soil sample. First, a

standard sample was prepared by growing a single clone containing the correct insert in the Luria-Bertani medium. The plasmid DNA was extracted and purified using the MiniBEST Plasmid Purification kit (Takara Bio Inc., Kusatsu, Shiga, Japan), and further quantified using Nanodrop 2000 (Thermo Fisher Scientific, Waltham, MA, USA). The standard sample was diluted in a 10-fold stepwise series and a standard curve was produced that covered a range of 102-108 copies of the template per assay. The assays were performed using the SYBR Premix Ex TaqTM Kit (Takara Bio Inc., Kusatsu, Shiga, Japan) with a 25-μL reaction mixture containing 12.5 μL of SYBR® Premix Ex TaqTM, 1 μL of the primer set (initial concentration of 10 μM each), 0.5 μL of BSA at 20 mg/mL initial concentration, and 1.0 μL of template containing approximately 3–9 ng of DNA. The same procedure was carried out for a blank, using ultrapure water instead of soil DNA extract as the template. The quantification of bacterial 16S rRNA genes and eukaryotic 18S rRNA genes was obtained by ealibrating data against the total DNA concentrations extracted and soil water content. Figure S9 at Supporting Information shows the detailed whole experimental procedure used in this study.

Data analysis. Statistical analyses were conducted in R (http://www.r-project.org/). The experiments were performed in a completely randomized design, with three replicates. Two-way analysis of variance (ANOVA) was performed. The mean values were compared by the Kruskal-Wallis test (p<0.05). Data are presented as means or medians with standard error bars (S.E.) or as means or medians with standard deviation bars (S.D.). The real-time quantitative PCR was compared by the Student's t-test (p < 0.05). To assess changes in the soil microbial community system network, we evaluated the occurrence of system modulation under untreated and treated soil samples *via* measurement of global network connectance (Cg_{Total}) related to selected microbial biomass and enzymatic activity traits as homeostatic signals. A systemic network connectance analysis was performed according to Amzallag, ⁶³ allowing us to assess

the homeostatic dimension (modulation and stability behavior) of the soil microbial community. Soil microbial community biomass and enzyme activity are indicators of soil quality, and these data are suitable to be analyzed as a network. Network theory has been used for analyzing data in ecology and plant physiology. $^{87-89}$ Network connectance was estimated using the correlation network model by assessing the normalized Person's correlation coefficient (r) among the selected parameters of soil microbial community biomass and enzyme activity followed by z transformation of r values according to equation [eq. 04): 63

$$Z = 0.5ln\left(\frac{1+|r|}{1-|r|}\right)$$
 [eq. 04]

Finally, we determine the global network connectance (Cg_{Total}) of selected paired parameters as the average of absolute z values as Amzallag. ⁶³

ASSOCIATED CONTENT

si Supporting Information

The Supporting Information is Available online.

Additional experimental methods, chemicals, characterization, hydrodynamic diameter, zeta potential, magnetic characterization, DFT calculations, mathematical modeling of release kinetics, soil characterization, and primers used in this study are available on Supporting Information. Additionally, the herbicidal activity was evaluated by the inhibition of photosystem II electron transport using a handheld chlorophyll fluorometer (Hansatech Instruments, UK). See Figure S10 in the Supporting Information.

Declaration of Competing Interest

The authors declare no conflict of interest.

577

Acknowledgments

The authors would like to thank CNPq, PROPP/UEMS, CAPES, and FAPESP for their 578 financial support. This study was financed in part by the Coordenação de Aperfeiçoamento de 579 Pessoal de Nível Superior - Brasil (CAPES) - Finance Code 001. M.S.P., A.R.L.C.; E.F.S.; and 580 R.G. also acknowledge the financial support provided by the National System of Photonics 581 Laboratories – Sisfóton/MCTI (CNPq grant numbers: 440214/2021-1 and 351485/2022-8). 582 R.G. would also like to thank São Paulo Research Foundation, FAPESP (Grant #2022/03219-583 2). This study was also financed in part by the PIBAP/UEMS (Resolução CEPE-UEMS nº 584 1.945, de 01/03/2018). We are grateful to Dra. V. Santos for the technical support. 585

586

587

References

- Crist, E.; Mora, C.; Engelman, R. The Interaction of Human Population, Food Production, and Biodiversity Protection. *Science* (1979) **2017**, 356 (6335), 260–264. https://doi.org/10.1126/science.aal2011.
- Shen, Y.; An, C.; Jiang, J.; Huang, B.; Li, N.; Sun, C.; Wang, C.; Zhan, S.; Li, X.; Gao, (2) 591 F.; Zhao, X.; Cui, H., Gooneratne, R.; Wang, Y. Temperature-Dependent Nanogel for 592 Pesticide Smart Delivery with Improved Foliar Dispersion and Bioactivity for Efficient 593 Multiple Pests. ACSNano 2022, 20622-20632. 594 16 (12),
- 595 https://doi.org/10.1021/acsnano.2c07517.
- Pontes, M. S.; Antunes, D. R.; Oliveira, I. P.; Forini, M. M. L.; Santos, J. S.; Arruda, G.
 J.; Caires, A. R. L.; Santiago, E. F.; Grillo, R. Chitosan/Tripolyphosphate
 Nanoformulation Carrying Paraquat: Insights on Its Enhanced Herbicidal Activity.
 Environ. Sci. Nano 2021, 8 (5), 1336–1351. https://doi.org/10.1039/D0EN01128B.

- 600 (4) Lima, P. H. C. de; Antunes, D. R.; Forini, M. M. de L.; Pontes, M. da S.; Mattos, B. D.;
- 601 Grillo, R. Recent Advances on Lignocellulosic-Based Nanopesticides for Agricultural
- Applications. Frontiers in Nanotech. 2021, 3.
- 603 https://doi.org/10.3389/fnano.2021.809329.
- 604 (5) Forini, M. M. L.; Pontes, M. S.; Antunes, D. R.; Lima, P. H. C. de; Santos, J. S.; Santiago,
- E. F.; Grillo, R. Nano-Enabled Weed Management in Agriculture: From Strategic Design
- to Enhanced Herbicidal Activity. Plant Nano Biol. 2022, 1, 100008.
- 607 https://doi.org/10.1016/j.plana.2022.100008.
- 608 (6) Adisa, I. O.; Pullagurala, V. L. R.; Peralta-Videa, J. R.; Dinkpa, C. O.; Elmer, W. H.;
- Gardea-Torresdey, J. L.; White, J. C. Recent Advances in Nano-Enabled Fertilizers and
- Pesticides: A Critical Review of Mechanisms of Action. *Environ. Sci. Nano* **2019**, *6* (7),
- 611 2002–2030. https://doi.org/10.1039/C9EN00265K
- 612 (7) Gomez, A.; Narayan, M.; Zhao, L., Jia, X., Bernal, R. A.; Lopez-Moreno, M. L.; Peralta-
- Videa, J. R. Effects of Nano-Enabled Agricultural Strategies on Food Quality: Current
- Knowledge and Future Research Needs. J. Hazard. Mater. 2021, 401, 123385.
- https://doi.org/10.1016/j.jhazmat.2020.123385.
- 616 (8) López-Cabeza, R.; Kah, M.; Grillo, R.; Koutný, M.; Salač, J.; Bílková, Z.; Eghbalinejad,
- M.; Hofman, J. Tebuconazole and Terbuthylazine Encapsulated in Nanocarriers:
- Preparation, Characterization and Release Kinetics. Environ. Sci. Nano 2022, 9 (4),
- 619 1427–1438. https://doi.org/10.1039/D1EN00981H.
- 620 (9) Wang, D.; Saleh, N. B.; Byro, A.; Zepp, R.; Sahle-Demessie, E.; Luxton, T. P.; Ho, K.
- T.; Burgess, R. M.; Flury, M.; White, J. C.; Su, C. Nano-Enabled Pesticides for
- Sustainable Agriculture and Global Food Security. *Nat. Nanotechnol* **2022**, *17* (4), 347–
- 623 360. https://doi.org/10.1038/s41565-022-01082-8.

- 624 (10) Mezacasa, A. V.; Queiroz, A. M.; Graciano, D. E.; Pontes, M. S.; Santiago, E. F.;
- Oliveira, I. P.; Lopez, A. J.; Casagrande, G. A.; Scherer, M. D.; dos Reis, D. D.; Oliveira,
- S. L.; Caires, A. R. L. Effects of Gold Nanoparticles on Photophysical Behaviour of
- 627 Chlorophyll and Pheophytin. J. Photochem. Photobiol. A Chem 2020, 389, 112252.
- 628 https://doi.org/10.1016/j.jphotochem.2019.112252.
- 629 (11) de Paiva Pinheiro, S. K.; Rangel Miguel, T. B. A.; Chaves, M. de M.; Barros, F. C. de
- F.; Farias, C. P.; de Moura, T. A.; Ferreira, O. P.; Paschoal, A. R.; Squza Filho, A. G.;
- de Castro Miguel, E. Silver Nanoparticles (AgNPs) Internalization and Passage through
- the Lactuca Sativa (Asteraceae) Outer Cell Wall. Funct. Plant Biology 2021, 48 (11),
- 633 1113. https://doi.org/10.1071/FP21161.
- 634 (12) Miguel, T. B. A. R.; Pinheiro, S. K. de P.; de Castro Miguel, E. Interaction of
- Nanomaterials with Biological Systems; In: Nascimento R. F.; Neto, V. O. S.; Fechine,
- P. B. A.; Freire, P. T. C. (eds) Nanomaterials and Nanotechnology. Materials Horizons:
- From Nature to Nanomaterials, Springer International Publishing: Singapore, 2021; pp
- 638 375–409. https://doi.org/10.1007/978-981-33-6056-3 12.
- 639 (13) Lowry, G. v.; Avellan, A.; Gilbertson, L. M. Opportunities and Challenges for
- Nanotechnology in the Agri-Tech Revolution. *Nat. Nanotechnol* **2019**, *14* (6), 517–522.
- https://doi.org/10.1038/s41565-019-0461-7.
- 642 (14) Liang, W.; Xie, Z.; Cheng, J.; Xiao, D.; Xiong, Q.; Wang, Q.; Zhao, J.; Gui, W. A Light-
- Triggered pH-Responsive Metal–Organic Framework for Smart Delivery of Fungicide
- to Control Sclerotinia Diseases of Oilseed Rape. ACS Nano 2021, 15 (4), 6987–6997.
- https://doi.org/10.1021/acsnano.0c10877.
- 646 (15) Wu, J.; Zhai, Y.; Monikh, F. A.; Arenas-Lago, D.; Grillo, R.; Vijver, M. G.; Peijnenburg,
- W. J. G. M. The Differences between the Effects of a Nanoformulation and a

- 648 Conventional Form of Atrazine to Lettuce: Physiological Responses, Defense
- Mechanisms, and Nutrient Displacement. J. Agric. Food Chem. 2021, 69 (42), 12527–
- 650 12540. https://doi.org/10.1021/acs.jafc.1c01382.
- 651 (16) Kah, M.; Weniger, A.-K.; Hofmann, T. Impacts of (Nano)Formulations on the Fate of
- an Insecticide in Soil and Consequences for Environmental Exposure Assessment.
- 653 Environ. Sci. Technol. **2016**, 50 (20), 10960–10967.
- https://doi.org/10.1021/acs.est.6b02477.
- 655 (17) Galhardi, J. A.; Luiz de Oliveira, J.; Ghoshal, S.; Fraceto, L. F. Soil Enzyme Responses
- 656 to Polymeric Nanopesticides: An Ecological Risk Analysis Approach to Promote
- Sustainable Agriculture. ACS Agricultural Sci. Technol. 2022, 2 (3), 443-452.
- https://doi.org/10.1021/acsagscitech.1c00234.
- 659 (18) Zhai, Y.; Abdolahpur Monikh, F.; Wu, J., Grillo, R.; Arenas-Lago, D.; Darbha, G. K.;
- Vijver, M. G.; Peijnenburg, W. J. G. M. Interaction between a Nano-Formulation of
- Atrazine and Rhizosphere Bacterial Communities: Atrazine Degradation and Bacterial
- 662 Community Alterations. *Environ. Sci. Nano* **2020**, 7 (11), 3372–3384.
- https://doi.org/10.1039/D0EN00638F.
- 664 (19) Bueno, V.; Wang, P.; Harrisson, O.; Bayen, S.; Ghoshal, S. Impacts of a Porous Hollow
- Silica Nanoparticle-Encapsulated Pesticide Applied to Soils on Plant Growth and Soil
- 666 Microbial Community. *Environ. Sci. Nano* **2022**, 9 (4), 1476–1488.
- 667 https://doi.org/10.1039/D1EN00975C.
- 668 (20) Takeshita, V.; Carvalho, L. B.; Galhardi, J. A.; Munhoz-Garcia, G. V.; Pimpinato, R. F.;
- Oliveira, H. C.; Tornisielo, V. L.; Fraceto, L. F. Development of a Preemergent
- Nanoherbicide: From Efficiency Evaluation to the Assessment of Environmental Fate

- and Risks to Soil Microorganisms. ACS Nanoscience Au 2022, 2 (4), 307–323.
- https://doi.org/10.1021/acsnanoscienceau.1c00055.
- 673 (21) Kah, M.; Navarro, D.; Schenkeveld, W.; Kookana, R. S.; Kirby, J. K.; Santra, S.; Ozcan,
- A. Fate of Copper in Soil: Effect of Agrochemical (Nano)Formulations and Soil
- 675 Properties. *Environ. Sci. Nano* **2022**, 9 (2), 653–662.
- 676 https://doi.org/10.1039/D1EN00213A.
- 677 (22) Kalra, R.; Conlan, X. A.; Goel, M. Lichen Allelopathy: A New Hope for Limiting
- 678 Chemical Herbicide and Pesticide Use. *Biocontrol. Sci. Technol.* **2021**, *31* (8), 773–796.
- https://doi.org/10.1080/09583157.2021.1901071.
- 680 (23) Romagni, J. G.; Meazza, G.; Nanayakkara, N. P. D.; Dayan, F. E. The Phytotoxic Lichen
- Metabolite, Usnic Acid, Is a Potent Inhibitor of Plant p -Hydroxyphenylpyruvate
- Dioxygenase. FEBS Lett **2000**, 480 (2–3) 301–305. https://doi.org/10.1016/S0014-
- 683 5793(00)01907-4.
- 684 (24) Latkowska, E.; Lechowski, Z.; Bialczyk, J.; Pilarski, J. Photosynthesis and Water
- Relations in Tomato Plants Cultivated Long-Term in Media Containing (+)-Usnic Acid.
- 586 J. Chem. Ecol. 2006, 32 (9), 2053–2066. https://doi.org/10.1007/s10886-006-9128-6.
- 687 (25) Gao, Y. Liu, W.; Wang, X.; Yang, L.; Han, S.; Chen, S.; Strasser, R. J.; Valverde, B.
- E.; Qiang, S. Comparative Phytotoxicity of Usnic Acid, Salicylic Acid, Cinnamic Acid
- and Benzoic Acid on Photosynthetic Apparatus of Chlamydomonas reinhardtii. Plant
- 690 *Physiol. Biochem.* **2018**, *128*, 1–12. https://doi.org/10.1016/j.plaphy.2018.04.037.
- 691 (26) Forini, M. M. L.; Antunes, D. R.; Cavalcante, L. A. F.; Pontes, M. S.; Biscalchim, É. R.;
- Sanches, A. O.; Santiago, E. F.; Fraceto, L. F.; Grillo, R. Fabrication and
- 693 Characterization of a Novel Herbicide Delivery System with Magnetic Collectability and

- Its Phytotoxic Effect on Photosystem II of Aquatic Macrophyte. J. Agric. Food Chem.
- 695 **2020**, 68 (40), 11105–11113. https://doi.org/10.1021/acs.jafc.0c03645.
- 696 (27) Gardia-Parège, C.; Kim Tiam, S.; Budzinski, H.; Mazzella, N.; Devier, M.-H.; Morin, S.
- Pesticide Toxicity towards Microalgae Increases with Environmental Mixture
- 698 Complexity. *Environ. Sci. Pollut. Research* **2022**, 29 (20), 29368–29381.
- 699 https://doi.org/10.1007/s11356-021-17811-w.
- 700 (28) Wang, D.; Saleh, N. B.; Byro, A.; Zepp, R.; Sahle-Demessie, E.; Luxton, T. P.; Ho, K.
- 701 T.; Burgess, R. M.; Flury, M.; White, J. C.; Su, C. Nano-Enabled Pesticides for
- Sustainable Agriculture and Global Food Security. Nat. Nanotechnol. 2022, 17 (4), 347–
- 703 360. https://doi.org/10.1038/s41565-022-01082-8.
- 704 (29) Preisler, A. C.; Pereira, A. E.; Campos, E. V.; Dalazen, G.; Fraceto, L. F.; Oliveira, H.
- 705 C. Atrazine Nanoencapsulation Improves Pre-emergence Herbicidal Activity against
- 706 Bidens Pilosa without Enhancing Long-term Residual Effect on Glycine Max. Pest
- 707 *Manag. Sci.* **2020**, 76 (1), 141–149. https://doi.org/10.1002/ps.5482.
- 708 (30) Assalin, M. R.; dos Santos, L. D. L.; Souza, D. R. C.; Rosa, M. A.; Duarte, R. C. R. M.;
- Castanha, R. F.; Donaire, P. P. R.; Durán, N. Ecotoxicity Evaluation: Preparation of
- Poly-ε-Caprolactone and Chitosan Nanoparticles as Carriers of Thiamethoxam Pesticide.
- 711 J. Phys. Conf. Ser. **2019**, 1323 (1), 012017. https://doi.org/10.1088/1742-
- 712 6596/1323/1/012017.
- 713 (31) Grillo, R.; Gallo, J.; Stroppa, D. G.; Carbó-Argibay, E.; Lima, R.; Fraceto, L. F.;
- Bañobre-López, M. Sub-Micrometer Magnetic Nanocomposites: Insights into the Effect
- of Magnetic Nanoparticles Interactions on the Optimization of SAR and MRI
- 716 Performance. ACS Appl. Mater. Interfaces 2016, 8 (39), 25777–25787.
- 717 https://doi.org/10.1021/acsami.6b08663.

- 718 (32) Bustamante-Torres, M.; Romero-Fierro, D.; Estrella-Nuñez, J.; Arcentales-Vera, B.;
- 719 Chichande-Proaño, E.; Bucio, E. Polymeric Composite of Magnetite Iron Oxide
- Nanoparticles and Their Application in Biomedicine: A Review. *Polymers (Basel)* **2022**,
- 721 *14* (4), 752. https://doi.org/10.3390/polym14040752.
- 722 (33) Grillo, R.; Mattos, B. D.; Antunes, D. R.; Forini, M. M. L.; Monikh, F. A.; Rojas, O. J.
- Foliage Adhesion and Interactions with Particulate Delivery Systems for Plant
- Nanobionics and Intelligent Agriculture. Nano Today 2021, 37, 101078.
- 725 https://doi.org/10.1016/j.nantod.2021.101078.
- 726 (34) Li, Y.; Xia, Y.; Liu, K.; Ye, K.; Wang, Q.; Zhang, S.; Huang, Y., Liu, H. Constructing
- 727 Fe-MOF-Derived Z-Scheme Photocatalysts with Enhanced Charge Transport:
- Nanointerface and Carbon Sheath Synergistic Effect. ACS Appl. Mater. Interfaces 2020,
- 729 12 (22), 25494–25502. https://doi.org/10.1021/acsami.0c06601.
- 730 (35) Wang, Y.; Zhang, J.; Balogun, M.-S.; Tong, Y.; Huang, Y. Oxygen Vacancy-Based
- Metal Oxides Photoanodes in Photoelectrochemical Water Splitting. *Materials Today*
- 732 Sustainability **2022**, 18, 100118. https://doi.org/10.1016/j.mtsust.2022.100118.
- 733 (36) Karimzadeh, I.; Aghazadeh, M.; Doroudi, T.; Ganjali, M. R.; Kolivand, P. H.
- Superparamagnetic Iron Oxide (Fe₃O₄) Nanoparticles Coated with PEG/PEI for
- Biomedical Applications: A Facile and Scalable Preparation Route Based on the
- 736 Cathodic Electrochemical Deposition Method. Adv. Physical Chemistry 2017, 2017, 1–
- 7. https://doi.org/10.1155/2017/9437487.
- 738 (37) Hammed, A.; Voronov, A.; Pryor, S. Scalable and Sustainable Synthesis of
- Superparamagnetic Iron Oxide Nanoparticles Using New Tubular Electrochemical
- 740 System. J. Appl. Electrochem. **2021**, 51 (7), 1093–1100. https://doi.org/10.1007/s10800-
- 741 021-01560-2.

- 742 (38) Berg, J. M.; Romoser, A.; Banerjee, N.; Zebda, R.; Sayes, C. M. The Relationship
- between PH and Zeta Potential of ~ 30 nm Metal Oxide Nanoparticle Suspensions
- Relevant to in Vitro Toxicological Evaluations. Nanotoxicology 2009, 3 (4), 276–283.
- 745 https://doi.org/10.3109/17435390903276941.
- 746 (39) Grillo, R.; Fraceto, L. F. Impacts of Magnetic Iron Oxide Nanoparticles in Terrestrial
- and Aquatic Environments. In: Williams, M. A. (ed) *Toxicology of Nanoparticles and*
- Nanomaterials in Human, Terrestrial and Aquatic Systems; Wiley, New Jersey, 2022;
- pp 147–164. https://doi.org/10.1002/9781119316329.ch7.
- 750 (40) Zugic, A.; Tadic, V.; Savic, S. Nano- and Microcarriers as Drug Delivery Systems for
- Usnic Acid: Review of Literature. Pharmaceutics 2020, 12 (2), 156.
- 752 https://doi.org/10.3390/pharmaceutics12020156
- 753 (41) Alpsoy, L.; Baykal, A.; Amir, Md.; Ülker, Z.; Nawaz, M. SPION@APTES@FA-
- PEG@Usnic Acid Bionanodrug for Cancer Therapy. J. Supercond. Nov. Magn. 2018, 31
- 755 (5), 1395–1401. https://doi.org/10.1007/s10948-017-4333-9.
- 756 (42) Harris, R. A.; Shumbula, P. M.; van der Walt, H. Analysis of the Interaction of
- 757 Surfactants Oleic Acid and Oleylamine with Iron Oxide Nanoparticles through
- 758 Molecular Mechanics Modeling. *Langmuir* **2015**, *31* (13), 3934–3943.
- 759 https://doi.org/10.1021/acs.langmuir.5b00671.
- 760 (43) Yang, K.; Peng, H.; Wen, Y.; Li, N. Re-Examination of Characteristic FTIR Spectrum
- of Secondary Layer in Bilayer Oleic Acid-Coated Fe₃O₄ Nanoparticles. *Appl. Surf. Sci.*
- **2010**, 256 (10), 3093–3097. https://doi.org/10.1016/j.apsusc.2009.11.079.
- 763 (44) Baykal, A.; Amir, Md.; Günerb, S.; Sözeri, H. Preparation and Characterization of
- SPION Functionalized via Caffeic Acid. J. Magn. Magn. Mater. 2015, 395, 199–204.
- 765 https://doi.org/10.1016/j.jmmm.2015.07.095.

- 766 (45) Villa, N. S.; Serra, G.; Bonoldi, L.; Assanelli, G.; Notari, M.; Lucotti, A.; Tommasini,
- M. Combining Micro-Infrared Reflection Absorption Spectroscopy with Density
- Functional Theory for Investigating the Adsorption of Organic Friction Modifiers on
- 769 Steel Surfaces. Vib. Spectrosc 2022, 121, 103403.
- 770 https://doi.org/10.1016/j.vibspec.2022.103403.
- 771 (46) Lan, Q.; Liu, C.; Yang, F.; Liu, S.; Xu, J.; Sun, D. Synthesis of Bilayer Oleic Acid-
- Coated Fe3O4 Nanoparticles and Their Application in PH-Responsive Pickering
- 773 Emulsions. J. Colloid Interface Sci. **2007**, 310 (1), 260–269.
- 774 https://doi.org/10.1016/j.jcis.2007.01.081.
- 775 (47) Cetin Cakmak, K.; Gülçin, İ. Anticholinergic and Antioxidant Activities of Usnic Acid-
- an Activity-Structure Insight. Toxicol. Rep. 2019, 6, 1273–1280.
- 777 https://doi.org/10.1016/j.toxrep.2019.11.003.
- 778 (48) Bilesky-José, N.; Maruyama, C.; Germano-Costa, T.; Campos, E.; Carvalho, L.; Grillo,
- R.; Fraceto, L. F.; de Lima, R. Biogenic α-Fe 2 O 3 Nanoparticles Enhance the Biological
- Activity of Trichoderma against the Plant Pathogen Sclerotinia Sclerotiorum. ACS
- 781 Sustain. Chem. 1 Eng. 2021, 9 (4), 1669–1683.
- https://doi.org/10.1021/acssuschemeng.0c07349.
- 783 (49) Akbari B; Tavandashti M; Zandrahimi M. Particle Size Characterization of
- Nanoparticles- a Practical Approach. *Iranian J. Mater. Sci. Eng.* **2011**, 8 (2), 48–56.
- 785 (50) Mircioiu, C.; Voicu, V.; Anuta, V.; Tudose, A.; Celia, C.; Paolino, D.; Fresta, M.;
- Sandulovici, R.; Mircioiu, I. Mathematical Modeling of Release Kinetics from
- Supramolecular Drug Delivery Systems. *Pharmaceutics* **2019**, *11* (3), 140.
- https://doi.org/10.3390/pharmaceutics11030140.

- 789 (51) Hall, C. Anomalous Diffusion in Unsaturated Flow: Fact or Fiction? Cem. Concr. Res.
- **2007**, *37* (3), 378–385. https://doi.org/10.1016/j.cemconres.2006.10.004.
- 791 (52) Kamran, M.; Ali, H.; Saeed, M. F.; Bakhat, H. F.; Hassan, Z.; Tahir, M.; Abbas, G.;
- Naeem, M. A.; Rashid, M. I.; Shah, G. M. Unraveling the Toxic Effects of Iron Oxide
- Nanoparticles on Nitrogen Cycling through Manure-Soil-Plant Continuum. *Ecotoxicol*.
- 794 Environ. Saf. **2020**, 205, 111099. https://doi.org/10.1016/j.ecoenv.2020.111099.
- 795 (53) Bhatia, Y.; Mishra, S.; Bisaria, V. S. Microbial β-Glucosidases: Cloning Properties, and
- 796 Applications. Crit. Rev. Biotechnol. 2002, 22 (4), 375–407.
- 797 https://doi.org/10.1080/07388550290789568.
- 798 (54) Kah, M.; Johnston, L. J.; Kookana, R. S.; Bruce, W.; Haase, A.; Ritz, V.; Dinglasan, J.;
- Doak, S.; Garelick, H.; Gubala, V. Comprehensive Framework for Human Health Risk
- Assessment of Nanopesticides. Nat. Nanotechnol. 2021, 16 (9), 955–964.
- 801 https://doi.org/10.1038/s41565-021-00964-7.
- 802 (55) Brookes, P. C.; Landman, A.: Pruden, G.; Jenkinson, D. S. Chloroform Fumigation and
- the Release of Soil Nitrogen: A Rapid Direct Extraction Method to Measure Microbial
- 804 Biomass Nitrogen in Soil. Soil Biol. Biochem. 1985, 17 (6), 837–842.
- 805 https://doi.org/10.1016/0038-0717(85)90144-0.
- 806 (56) Margalef, O.; Sardans, J.; Fernández-Martínez, M.; Molowny-Horas, R.; Janssens, I. A.;
- Ciais, P.; Goll, D.; Richter, A.; Obersteiner, M.; Asensio, D.; Peñuelas, J. Global Patterns
- of Phosphatase Activity in Natural Soils. Sci. Rep. 2017, 7 (1), 1337.
- https://doi.org/10.1038/s41598-017-01418-8.
- 810 (57) Rizzello, C. G.; Curiel, J. A.; Nionelli, L.; Vincentini, O.; di Cagno, R.; Silano, M.;
- Gobbetti, M.; Coda, R. Use of Fungal Proteases and Selected Sourdough Lactic Acid

- Bacteria for Making Wheat Bread with an Intermediate Content of Gluten. Food
- 813 *Microbiol.* **2014**, *37*, 59–68. https://doi.org/10.1016/j.fm.2013.06.017.
- 814 (58) Caldwell, B. A. Enzyme Activities as a Component of Soil Biodiversity: A Review.
- 815 *Pedobiologia* (*Jena*) **2005**, 49 (6), 637–644.
- https://doi.org/10.1016/j.pedobi.2005.06.003.
- 817 (59) Kah, M.; Walch, H.; Hofmann, T. Environmental Fate of Nanopesticides: Durability,
- Sorption and Photodegradation of Nanoformulated Clothianidin. Environ. Sci. Nano
- **2018**, *5* (4), 882–889. https://doi.org/10.1039/C8EN00038G.
- 820 (60) Souza, G. M.; do Amaral, M. N. Emergent Properties and Stability in Hierarchical
- Biosystems: There Is No Privileged Level of Causation. In: Wegner, L.; Lüttge, U. (eds)
- 822 Emergence and Modularity in Life Sciences; Springer International Publishing: Cham,
- 2019; pp 217–234. https://doi.org/10.1007/978-3-030-06128-9 10.
- 824 (61) Wegner, L. H. Modularity Versus Emergence: How to Cope with Complexity in Whole-
- Plant Physiology? In: Wegner, Lt; Lüttge, U. (eds) Emergence and Modularity in Life
- Sciences; Springer International Publishing: Cham, 2019; pp 75–95.
- https://doi.org/10.1007/978-3-030-06128-9 4.
- 828 (62) Gomes, S. L. L., Campos, E. V. R.; Fraceto, L. F.; Grillo, R.; Scott-Fordsmand, J. J.;
- Amorim, M. J. B. High-Throughput Transcriptomics Reveals the Mechanisms of
- Nanopesticides Nanoformulation, Commercial Formulation, Active Ingredient -
- Finding Safe and Sustainable-by-Design (SSbD) Options for the Environment. *Environ*.
- 832 *Sci. Nano* **2022**, *9* (6), 2182–2194. https://doi.org/10.1039/D1EN00735A.
- 833 (63) Amzallag, G. N. Data Analysis in Plant Physiology: Are We Missing the Reality? *Plant*
- 834 *Cell Environ.* **2001**, 24 (9), 881–890. https://doi.org/10.1046/j.1365-3040.2001.00742.x.

- 835 (64) Amzallag, G. N. Maturation of Integrated Functions during Development. I.
- Modifications of the Regulatory Network during Transition Periods in *Sorghum Bicolor*.
- 837 Plant Cell Environ. **2001**, 24 (3), 337–345. https://doi.org/10.1046/j.1365-
- 838 3040.2001.00675.x.
- 839 (65) Kültz, D. Defining Biological Stress and Stress Responses Based on Principles of
- Physics. J. Exp. Zool. A Ecol. Integr. Physiol. 2020, 333 (6), 350–358.
- https://doi.org/10.1002/jez.2340.
- 842 (66) Santiago, E. F.; Pontes, M. S.; Arruda, G. J.; Caires, A. R. L.; Colbeck, I.; Maldonado-
- Rodriguez, R.; Grillo, R. Understanding the Interaction of Nanopesticides with Plants.
- In: Fraceto, L. F.; Castro, V. L. S. S.; Grillo, R.; Ávita, D. Oliveira, H. C.; Lima, R.
- 845 (eds) Nanopesticides; Springer International Publishing: Cham, 2020; pp 69–109.
- https://doi.org/10.1007/978-3-030-44873-8 4.
- 847 (67) Bertolli, S.; Vítolo, H.; Souza, G. Network Connectance Analysis as a Tool to
- Understand Homeostasis of Plants under Environmental Changes. *Plants* **2013**, *2* (3),
- 849 473–488. https://doi.org/10.3390/plants2030473.
- 850 (68) Antonenko, Y. N., Khailova, L. S.; Rokitskaya, T. I.; Nosikova, E. S.; Nazarov, P. A.;
- Luzina, O. A.; Salakhutdinov, N. F.; Kotova, E. A. Mechanism of Action of an Old
- Antibiotic Revisited: Role of Calcium Ions in Protonophoric Activity of Usnic Acid.
- 853 Biochim. Biophy. Acta (BBA) Bioenergetics **2019**, 1860 (4), 310–316.
- https://doi.org/10.1016/j.bbabio.2019.01.005.
- 855 (69) Pandit, S.; Rahimi, S.; Derouiche, A.; Boulaoued, A.; Mijakovic, I. Sustained Release of
- Usnic Acid from Graphene Coatings Ensures Long Term Antibiofilm Protection. Sci.
- 857 Rep. **2021**, 11 (1), 9956. https://doi.org/10.1038/s41598-021-89452-5.

- 858 (70) Maciąg-Dorszyńska, M.; Węgrzyn, G.; Guzow-Krzemińska, B. Antibacterial Activity of
- Lichen Secondary Metabolite Usnic Acid Is Primarily Caused by Inhibition of RNA and
- 860 DNA Synthesis. *FEMS Microbiol. Lett.* **2014**, *353* (1), 57–62.
- https://doi.org/10.1111/1574-6968.12409.
- 862 (71) Zhang, X.; Xu, Z.; Qian, X.; Lin, D.; Zeng, T.; Filser, J.; Li, L.; Kah, M. Assessing the
- Impacts of Cu(OH) 2 Nanopesticide and Ionic Copper on the Soil Enzyme Activity and
- Bacterial Community. J. Agric. Food. Chem. 2020, 68 (11), 3372–3381.
- https://doi.org/10.1021/acs.jafc.9b06325.
- 866 (72) Grillo, R.; Fraceto, L. F.; Amorim, M. J. B.; Scott-Fordsmand, J. J.; Schoonjans, R.;
- Chaudhry, Q. Ecotoxicological and Regulatory Aspects of Environmental Sustainability
- 868 of Nanopesticides. *J. Hazard. Mater.* **2021**, 404, 124148.
- https://doi.org/10.1016/j.jhazmat.2020.124148
- 870 (73) White, J. C.; Gardea-Torresdey, J. Achieving Food Security through the Very Small.
- Nat. Nanotechnol. 2018, 13 (8), 627–629. https://doi.org/10.1038/s41565-018-0223-y.
- 872 (74) Su, Y.; Zhou, X.; Meng, H., Xia, T.; Liu, H.; Rolshausen, P.; Roper, C.; McLean, J. E.;
- Zhang, Y.; Keller, A. A.; Jassby, D. Cost-Benefit Analysis of Nanofertilizers and
- Nanopesticides Emphasizes the Need to Improve the Efficiency of Nanoformulations for
- 875 Widescale Adoption. *Nat. Food* **2022**, *3* (12), 1020–1030.
- 876 https://doi.org/10.1038/s43016-022-00647-z.
- 877 (75) The IUPAC Compendium of Chemical Terminology; Gold, V., Ed.; International Union
- of Pure and Applied Chemistry (IUPAC): Research Triangle Park, NC, 2019.
- https://doi.org/10.1351/goldbook.

- 880 (76) Gomollón-Bel, F. Ten Chemical Innovations That Will Change Our World: IUPAC
- Identifies Emerging Technologies in Chemistry with Potential to Make Our Planet More
- Sustainable. Chem. Inter. **2019**, 41 (2), 12–17. https://doi.org/10.1515/ci-2019-0203.
- 883 (77) Brandão, A. S.; Gonçalves, A.; Santos, J. M. R. C. A. Circular Bioeconomy Strategies:
- From Scientific Research to Commercially Viable Products. J. Clean. Prod. 2021, 295,
- 885 126407. https://doi.org/10.1016/j.jclepro.2021.126407.
- 886 (78) Gilbertson, L. M.; Vikesland, P. J. Inspiring a Nanocircular Economy. Environ. Sci.
- 887 Nano **2022**, 9 (3), 839–840. https://doi.org/10.1039/D2EN90005
- 888 (79) Holzwarth, U.; Gibson, N. The Scherrer Equation versus the "Debye-Scherrer Equation."
- Nat. Nanotechnol. **2011**, 6 (9), 534–534. https://doi.org/10.1038/nnano.2011.145.
- 890 (80) Dini, G.; Ueji, R.; Najafizadeh, A.; Monir-Vaghefi, S. M. Flow Stress Analysis of TWIP
- Steel via the XRD Measurement of Dislocation Density. *Mater. Sci. Eng. A* **2010**, *527*
- 892 (10–11), 2759–2763. https://doi.org/10.1016/j.msea.2010.01.033.
- 893 (81) Chircov, C.; Ștefan, R.-E.; Dolete, G.; Andrei, A.; Holban, A. M.; Oprea, O.-C.; Vasile,
- B. S.; Neacşu, I. A.; Tihauan, B. Dextran-Coated Iron Oxide Nanoparticles Loaded with
- 895 Curcumin for Antimicrobial Therapies. *Pharmaceutics* **2022**, *14* (5), 1057.
- 896 https://doi.org/10.3390/pharmaceutics14051057.
- 897 (82) Mendyk Å; Jachowicz R. Unified Methodology of Neural Analysis in Decision Support
- 898 Systems Built for Pharmaceutical Technology. Expert Syst. Applications 2007, 32,
- 899 1124–1131.
- 900 (83) Hamidat, M.; Barakat, M.; Ortet, P.; Chanéac, C.; Rose, J.; Bottero, J.-Y.; Heulin, T.;
- Achouak, W.; Santaella, C. Design Defines the Effects of Nanoceria at a Low Dose on

- Soil Microbiota and the Potentiation of Impacts by the Canola Plant. Environ. Sci.
- 903 *Technol.* **2016**, *50* (13), 6892–6901. https://doi.org/10.1021/acs.est.6b01056.
- 904 (84) Ge, Y.; Schimel, J. P.; Holden, P. A. Identification of Soil Bacteria Susceptible to TiO 2
- 905 and ZnO Nanoparticles. Appl. Environ. Microbiol. 2012, 78 (18), 6749–6758.
- 906 https://doi.org/10.1128/AEM.00941-12.
- 907 (85) Tabatabai, M. A. Soil Enzymes; In: Weaver, R. W.; Augle, S.; Bottomly, P. J.; Bezdicek,
- 908 D.; Smith, S.; Tabatabai, A.; Wollum, A. (Eds.), Methods of soil analysis. Part 2.
- 909 Microbiological and biochemical properties. Soil Science Society of America Press:
- 910 Madison, 1994; pp 775–833. https://doi.org/10.2136/sssabookser5.2.c37.
- 911 (86) Feng, Y.; Lin, X.; Zhu, J.; Jia, Z. A Phototrophy-Driven Microbial Food Web in a Rice
- 912 Soil. J. Soils Sediments **2011**, 11 (2), 301–311 https://doi.org/10.1007/s11368-010-
- 913 0303-6.
- 914 (87) Souza, G. M.; Lüttge, U. Stability as a Phenomenon Emergent from Plasticity-
- Complexity–Diversity in Eco-Physiology; In Lüttge, U.; Beyschlag, W. (eds) Progress
- in Botany, Vol 76, Springer International Publishing: Cham. 2015; pp 211-239.
- 917 https://doi.org/10.1007/978-3-319-08807-5_9.
- 918 (88) Pontes, M. S., Grillo, R.; Graciano, D. E.; Falco, W. F.; Lima, S. M.; Caires, A. R. L.;
- 919 Andrade, L. H. C.; Santiago, E. F. How Does Aquatic Macrophyte Salvinia Auriculata
- Respond to Nanoceria upon an Increased CO₂ Source? A Fourier Transform-Infrared
- Photoacoustic Spectroscopy and Chlorophyll a Fluorescence Study. *Ecotoxicol. Environ.*
- 922 Saf. **2019**, 180, 526–534. https://doi.org/10.1016/j.ecoenv.2019.05.041.
- 923 (89) Pontes, M. S.; Graciano, D. E.; Antunes, D. R.; Santos, J. S.; Arruda, G. J.; Botero, E.
- 924 R.; Grillo, R.; Lima, S. M.; Andrade, L. H. C.; Caires, A. R. L.; Santiago, E. F. In Vitro
- and in vivo Impact Assessment of Eco-Designed CuO Nanoparticles on Non-Target

Aquatic Photoautotrophic Organisms. *J. Hazard. Mater.* **2020**, *396*, 122484. https://doi.org/10.1016/j.jhazmat.2020.122484.

